GeoScienceWorld
Lithosphere
Volume 2020, Article ID 2298288, 22 pages
https://doi.org/10.2113/2020/2298288

Lithosphere

Research Article

Late Cretaceous to Paleocene Tectonometamorphic Evolution of the Blanchard River Assemblage, Southwest Yukon: New Insight into the Terminal Accretion of Insular Terranes in the Northern Cordillera

Lianna Vice,[1] **H. Daniel Gibson**,[1] **and Steve Israel**[2]

[1]*Department of Earth Science, Simon Fraser University, 8888 University Drive, Burnaby, British Columbia, Canada V5A 1S6*
[2]*Yukon Geological Survey, PO Box 2703(K-14), Whitehorse, Yukon, Canada Y1A 2C6*

Correspondence should be addressed to Lianna Vice; liannavice@gmail.com

Received 13 February 2020; Revised 18 June 2020; Accepted 22 July 2020; Published 21 September 2020

Academic Editor: Tamer S. Abu-Alam

The Intermontane-Insular terrane boundary stretches over 2000 kilometers from British Columbia to Alaska in the western Cordillera. Juxtaposed between these terranes is a series of Jura-Cretaceous basinal and arc assemblages that record a complicated and contested tectonic evolution related to the Mesozoic-Paleocene accretionary history of northwestern North America. In southwest Yukon, west-verging thrust faults facilitated structural stacking of the Yukon-Tanana terrane over these basinal assemblages, including the Early Cretaceous Blanchard River assemblage. These previously undated compressional structures are thought to be related to the final collapse of the Jura-Cretaceous basins and the tectonic burial of the Blanchard River assemblage resulting in amphibolite facies metamorphism. New in situ U-Th-Pb monazite ages record at least three tectonic events: (1) the tectonic burial of the Blanchard River assemblage to amphibolite facies conditions between 83 and 76 Ma; (2) peak burial was followed by regional exhumation at ca. 70-68 Ma; and (3) intense heating and ca. 63-61 Ma low-pressure contact metamorphism attributed to the intrusion of the voluminous Ruby Range suite, which is part of the northern Coast Mountains batholith. The tectonometamorphic evolution recorded in the Blanchard River assemblage can be correlated to tectonism within southwest Yukon and along the length of the Insular-Intermontane boundary from western British Columbia through southwestern Yukon and Alaska. In southwest Yukon, these results suggest an asymmetric final collapse of Jura-Cretaceous basins during the Late Cretaceous, which relates to the terminal accretion of the Insular terranes as they moved northward.

1. Introduction

Since Devonian time, convergent margin tectonism has defined the architecture of the western margin of Laurentia, resulting in the accretion of allochthonous terranes progressing from the late Paleozoic-early Mesozoic into the early Cenozoic [1–10]. In the northern Cordillera, accretion began with the Intermontane terranes (Slide Mountain, Yukon-Tanana, Quesnel, Stikine, Cache Creek, and Bridge River terranes) from the Triassic (possibly as early as Late Permian) into the Middle Jurassic ([7, 8, 10] and references therein), followed by the accretion of Insular terranes that included Wrangellia and Alexander terrane (Figure 1) [2, 10–15].

The precise timing and mechanisms for accretion of the northern Canadian-Alaskan-Insular terranes against the western Laurentian margin are contentious. Two principal and contrasting models exist to reconcile the accretionary history of the Insular terranes, which include an initial Middle Jurassic [11, 12, 16–18] and final (terminal) mid- to Late Cretaceous accretion and/or collision [2, 14, 15, 19–25], or a single accretionary event from the Late Jurassic into the Cretaceous [26, 27]. Despite their differences, both models do agree that components of the Insular terranes did not terminally accrete until mid- to Late Cretaceous time.

Regardless of which model is favored there remains an additional discrepancy related to the final accretion of the

Insular terranes along the western Cordillera through British Columbia (BC), Yukon, and into Alaska. Specifically, during the Cretaceous there is up to 15 million years difference in ages of compressional events interpreted to have accommodated final accretion in west-central BC/southeast Alaska and south-central Alaska [19, 21, 25]. Evidence for contractional tectonism related to terminal accretion of the Insular terranes in west-central BC and southeastern Alaska is constrained to ca. 100-90 Ma [17, 19, 21]; however, in south-central Alaska, similar structural processes related to convergent tectonism attributed to Insular accretion did not occur until 85-75 Ma [25]. To investigate this dichotomy, researchers have focused on the geologic relationships found within Jurassic-Cretaceous overlap assemblages situated between the Intermontane and Insular terranes (e.g., Kahiltna, Nutzotin, Dezadeash/Kluane schist, Gravina, and Tyaughton-Methow; Figure 1) [12, 14, 21, 28, 29].

Importantly, the deformation and metamorphism recorded within the Jura-Cretaceous basinal assemblages can be directly attributed to the tectonic interaction between the Insular and Intermontane terranes and therefore can be used to constrain the timing of terminal accretion for the Insular terranes. Within Alaska and southwest Yukon, a series of these basinal assemblages are located between components of the Intermontane and Insular terranes that are bounded by the Denali, Tatshenshini, and Shakwak faults (Figures 1 and 2). Note that although we are calling it *terminal accretion*, the exact nature of the collapse of these Jura-Cretaceous basins is not fully understood. It is still equivocal whether actual subduction of oceanic lithosphere flooring the basins was directly involved in all or some of their closure, and if so, the polarity of that subduction is also contested as described above. Within the Cretaceous timeframe of the current study, *terminal accretion* is intended to represent the final collision and suturing of Insular terranes with the previously accreted Intermontane terranes.

The Jura-Cretaceous basinal assemblages in southwest Yukon include the Dezadeash Formation, the Kluane schist, and the newly defined Blanchard River and Vand Creek assemblages [32]. These assemblages have been variably deformed and metamorphosed up to amphibolite facies conditions [30, 31, 33–36]. The tectonic history of this region is not well understood as there have been limited detailed studies focused on the tectonometamorphic processes that have affected these rocks. Additionally, many of the crucial contacts between these units are obscured by the intrusion of Paleogene plutons, making it difficult to examine key relationships. The Blanchard River assemblage is penetratively deformed and contains high-grade metamorphic assemblages, making it an optimal candidate for geochronologic, structural, and metamorphic analyses to better characterize the tectonometamorphic evolution of this region.

This study documents the timing of deformation and metamorphism that has affected the Blanchard River assemblage and the overlying Yukon-Tanana terrane by linking in situ U-Pb monazite geochronology with observed structural and metamorphic textures. From this data, we have defined three main metamorphic events and two deformation events that are interpreted to be the product of late Mesozoic accretion of the Insular terranes within the northern Canadian-Alaskan Cordillera. The tectonic events recorded in southwest Yukon, described herein, support the hypotheses of Late Cretaceous to Paleocene crustal thickening and exhumation along the Intermontane-Insular boundary as part of the northern continuation of the Coast Mountains orogen.

2. Geological Background

2.1. Yukon-Tanana Terrane. The Intermontane terranes in southwest Yukon are largely represented by Yukon-Tanana terrane, which comprises polydeformed and metamorphosed Neoproterozoic to Devonian siliciclastic, volcanic, and carbonate rocks assigned to the Snowcap assemblage [6, 9, 31, 37]. The Yukon-Tanana terrane makes up much of central Yukon and has a long deformation history that has evolved through rifting and accretionary processes from the Devonian to its final accretion by Middle Jurassic time [2, 6, 7, 9, 37, 38]. These rocks record major metamorphism and deformation from the latest Triassic to earliest Jurassic [39–44].

2.2. Wrangellia and Alexander Terrane. The Insular terranes most relevant to this study include the Alexander terrane and Wrangellia, which make up a significant portion of the western edge of the Canadian-Alaskan Cordillera extending over 2000 km (Figure 1). In southwest Yukon, Alexander terrane is made up of siliciclastic, carbonate, and volcanic rocks ranging in age from Neoproterozoic to Upper Triassic [45, 46]. Northern Wrangellia is mostly characterized by late Paleozoic volcanic and sedimentary rocks overlain by Late Triassic flood basalt and sedimentary rocks [31, 46–49]. These two terranes shared a geologic history as far back as the Middle Pennsylvanian, possibly latest Devonian [46, 50, 51]. Thus, Alexander terrane and Wrangellia will be treated as a contiguous entity during the Mesozoic history documented in this study. In the northern Cordillera, Insular terrane rocks are juxtaposed with the Jura-Cretaceous basinal assemblages and Yukon-Tanana terrane along the Denali fault, a prominent structure that has accommodated 300 to 400 km of dextral strike slip displacement from the latest Cretaceous to present (Figure 1) [33, 52–54].

2.3. Jura-Cretaceous Basinal Assemblages. Within southwest Yukon, several Jura-Cretaceous basinal assemblages are fault bounded between the Yukon-Tanana terrane to the east and the Insular terranes to the west. These assemblages include the Dezadeash Formation (fossil ages of Oxfordian to Valanginian [33]; zircon maximum depositional age of ca. 148-147 Ma [55]), the Vand Creek assemblage (latest Jurassic [32]), the Blanchard River assemblage (Early Cretaceous [32]), and the Kluane schist (maximum depositional age of ca. 94 Ma [30]) (Figure 1). As few studies have addressed these basinal assemblages in detail, there is a limited understanding of their relationship to each other and the faults that separate them, which include the Shakwak fault, the Tatshenshini shear zone, the newly defined Kluhini River thrust (this study, [32]), and the Denali fault (Figure 1). Additionally, contacts and other primary geologic relationships are obscured in these basinal assemblages as significant portions

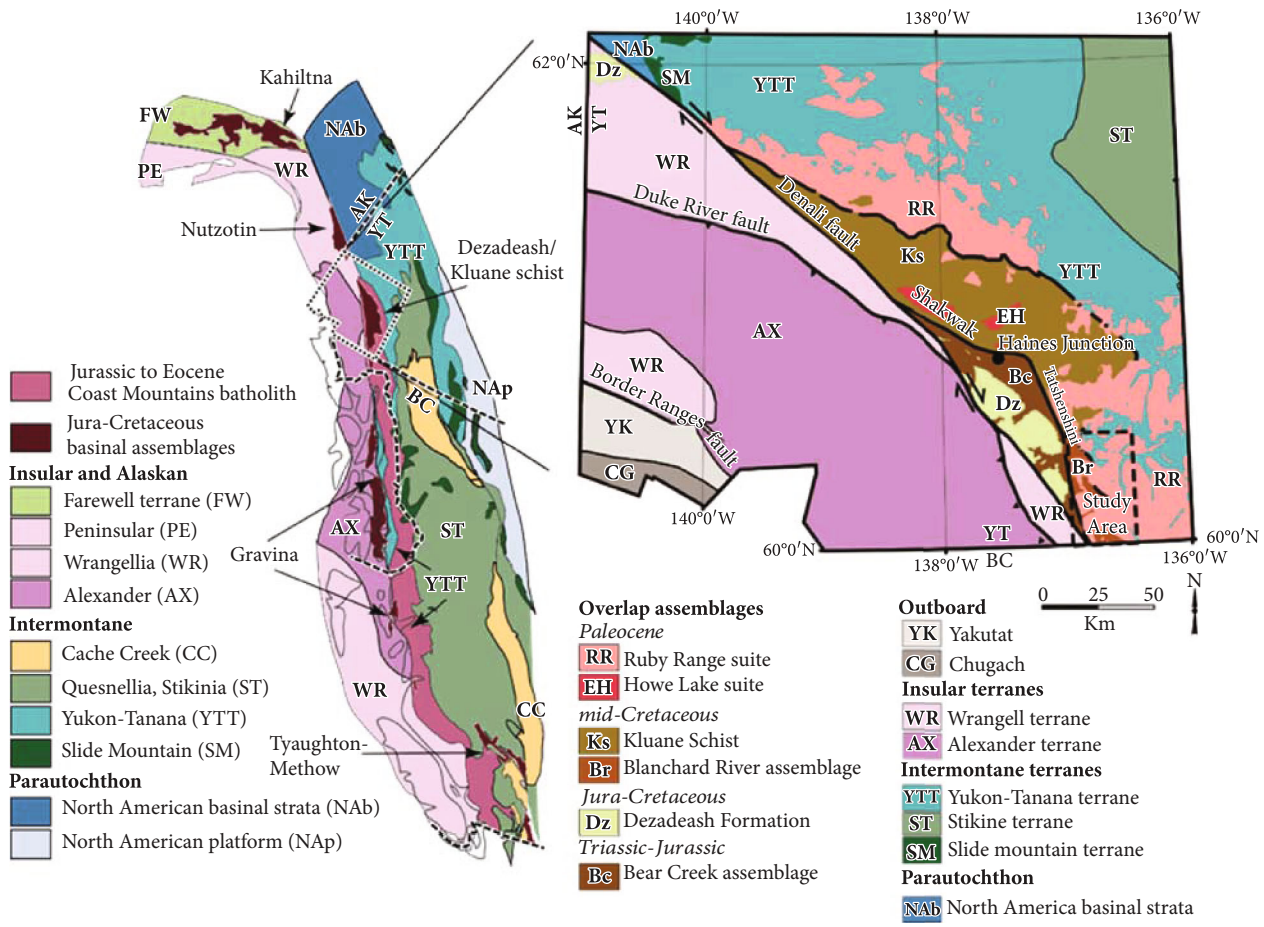

FIGURE 1: Terrane map of the western Canadian and Alaskan Cordillera including the Coast Mountains batholith. Jura-Cretaceous basinal assemblages are highlighted from southwestern BC into Alaska. The inset map shows the regional geology of southwestern Yukon including the Jura-Cretaceous basinal assemblages juxtaposed between the Insular and Intermontane terranes. The dashed line box in the lower right portion of the map shows the location of the study area (Figure 2). Abbreviations: YT: Yukon Territory; BC: British Columbia; AK: Alaska. The terrane map was modified from Israel et al. [30]; inset map was modified from Nelson et al. [9] and Bordet et al. [31].

have undergone intense deformation and metamorphism and have been intruded by post-deformation plutons of the Coast Mountains arc. Notably, in southwest Yukon, these plutons include the voluminous intermediate to felsic intrusions of the Paleocene to Eocene Ruby Range suite (64-51 Ma; Figures 1 and 2) [56–58].

2.3.1. Dezadeash Formation. The Dezadeash Formation is an ~3000 m thick package of Late Jurassic to Early Cretaceous metasiliciclastic rock deposited as a flysch sequence proximal to the Coast Mountains arc that has been regionally metamorphosed to at least greenschist facies, although lower grades are present [33, 36, 55]. Several structural features are recorded in the Dezadeash Formation, the oldest of which are pre-106 Ma asymmetric folds that are overturned towards the east and locally transfer laterally into thrust faults [33]. Younger, southwest-directed thrusting that occurred between 70 and 50 Ma places the Kluane schist over the Dezadeash Formation [33]. Superimposed on early structures are post-56 Ma, open folds trending to the west-northwest, which formed in response to mid-Cenozoic right-lateral shearing along the Shakwak fault zone (Figure 1) [33, 59].

2.3.2. The Kluane Schist. The Kluane schist is an early-Late Cretaceous package of deformed, amphibolite facies metasedimentary rock originally deposited along the western edge of the Yukon-Tanana terrane [30, 34, 35]. Metamorphism of the Kluane schist is characterized by two events: Late Cretaceous regional amphibolite facies metamorphism and deformation (~8 kbar and 500°C), followed by decompression (~3.5 kbar) and contact metamorphism (550°C) within a 5-6 km wide aureole that is associated with the intrusion of the Paleocene to Eocene Ruby Range suite [34, 35]. Some zircon grains in the Kluane schist have ca. 82 Ma metamorphic overgrowths that grew during crustal thickening as a result of thrusting and burial beneath the Yukon-Tanana terrane (Israel et al., 2011). Structures associated with thrusting are crosscut by ca. 70 Ma dikes [30].

3. Geology of the Blanchard River Area

3.1. Lithology. The Blanchard River area is characterized by four main rock units: (1) the Yukon-Tanana terrane; (2) the Vand Creek assemblage; (3) the Blanchard River assemblage; and (4) the Ruby Range suite (Figure 2).

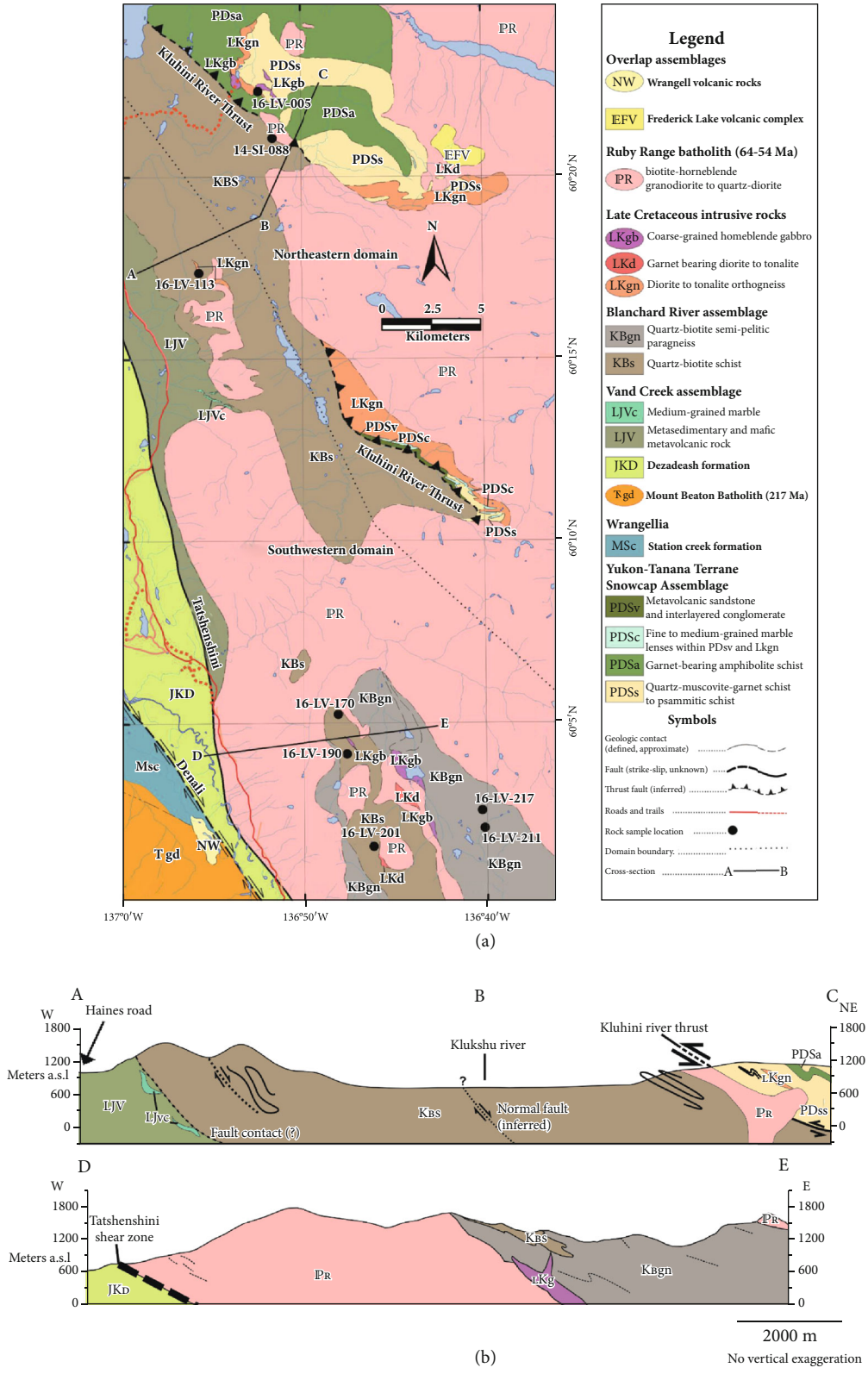

FIGURE 2: (a) Bedrock geology map and legend of the study area (modified from [31]). Sample locations for which U-Th-Pb analyses were carried out are shown. (b) Geological cross-sections through the Blanchard River area; locations and legend are specified in panel (a). a.s.l.: above sea level.

The Yukon-Tanana terrane is characterized by upper greenschist to amphibolite facies pelitic and semipelitic schist, amphibolite schist, metavolcanic-metavolcaniclastic schist, and marble (Figure 3). These rocks are assigned to the Snowcap assemblage based on their lithological and textural characteristics [31] and have undergone at least 4 phases of deformation, two of which are discussed in more detail below.

The informally named Vand Creek assemblage is characterized by green-black serpentinized hornblende metagabbro, fine-grained chloritic metabasite, chlorite schist, marble, quartzite, and phyllite. The relationships between the different lithological units are uncertain due to a lack of exposure. Rocks of the Vand Creek assemblage are lithologically distinct from those of the overlying Blanchard River assemblage and Yukon-Tanana terrane and appear to preserve lower grade assemblages indicative of greenschist facies metamorphism [32].

The Blanchard River assemblage is characterized by intensely deformed and interlayered units of quartz-biotite pelitic schist and quartz-biotite psammitic schist that have been metamorphosed to amphibolite facies conditions. This package of rocks is ~5-6 km thick, and despite intense deformation, primary depositional features such as bedding and graded bedding are locally visible parallel to the penetrative foliation (Figure 4). Within the southernmost part of the study area, the Blanchard River assemblage consists primarily of pelitic paragneiss, which contains interstitial lozenges of leucosome, often found in close proximity to contacts with Late Cretaceous intrusions, and to a lesser degree the Ruby Range suite (Figure 4). Late Cretaceous intrusions (78-76 Ma) within rocks of Yukon-Tanana terrane and Blanchard River assemblage consist of medium- to coarse-grained gabbro, dioritic to tonalitic orthogneiss, and garnet-bearing diorite to tonalite (Figure 2).

The Ruby Range suite intrudes much of the study area and consists of Paleocene to Eocene, medium- to coarse-grained biotite-hornblende granodiorite to quartz diorite. These intrusions crosscut the penetrative deformation found within the Snowcap, Vand Creek, and Blanchard River assemblages. In general, there is no discernable ductile fabrics within rocks of the Ruby Range suite, except when it is found within the hanging wall of the Tatshenshini shear zone where the alignment of biotite and hornblende defines a strong foliation parallel to the northwest-striking shear zone.

3.2. Structure. For the purposes of this study, we focus on the Cretaceous and younger deformation that has affected the region since the deposition of the Blanchard River assemblage. Pre-Cretaceous deformation events preserved in the Yukon-Tanana terrane rocks relate to an earlier geological history (e.g., [40–44]) and are not considered further. For ease of discussion, we have separated the study area into a northeastern and southwestern domain (Figure 2). Two distinct deformation phases have been identified (D_T and D_{T+1}). The penetrative transposition foliation (S_T) characterizes the first phase of deformation (D_T) within the Blanchard River assemblage. Structural data plotted in lower hemisphere equal area projections from the northeastern and southwestern domains are included in Supplementary 1.

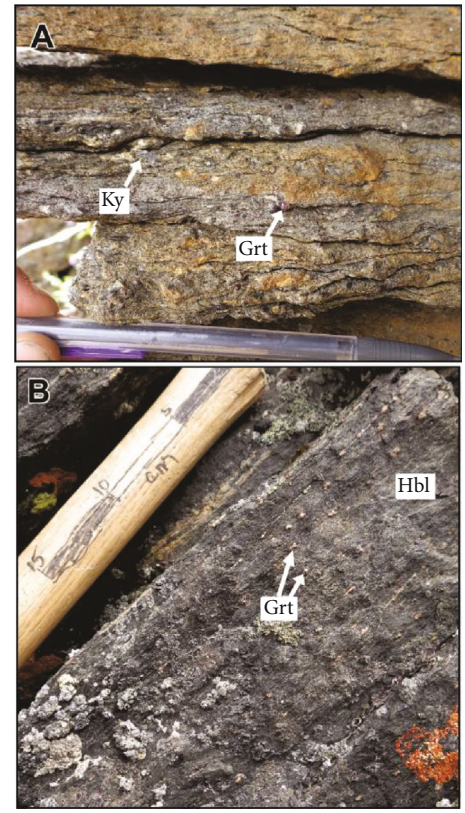

Figure 3: Photographs of rocks showing characteristics of Yukon-Tanana terrane units in the hanging wall of the Kluhini River thrust near sample 16-LV-005 (Figure 2(a)). (a) Garnet-kyanite-biotite-muscovite schist from unit PDSs. Kyanite is aligned along the S_T foliation; pencil for scale is ~15 cm in length. (b) Well-foliated garnet-amphibolite of the unit PDsa.

3.2.1. D_T. The penetrative transposition foliation (S_T) in the study area strikes northwest and dips moderately to the northeast (Supplementary 1) and is defined by the alignment of micaceous minerals. In the Snowcap assemblage S_T parallels the axial surface of tight southwest-verging folds (F_T) that refold an Early Jurassic penetrative fabric [44]. In the Blanchard River assemblage, these southwest-verging folds are also tight to isoclinal (F_T) and transpose the original bedding (S_0; Figure 5(a)).

In the northeastern domain, the penetrative foliation (S_T) in the Snowcap assemblage, Blanchard River assemblage, and Late Cretaceous orthogneiss has a consistent west-northwest strike that dips moderately to the north-northeast. In this domain, the Kluhini River thrust has placed the Yukon-Tanana terrane on top of the Blanchard River assemblage (Figure 2). The fault parallels the S_T foliation and in places is crosscut by the intrusion of the Ruby Range suite. Shear sense indicators within the S_T foliation proximal to the fault and congruent to F_T folding indicate a top to the southwest sense of shear (Figure 5(d)).

In the southwestern domain, the Blanchard River assemblage sits above the metasedimentary/metavolcanic rocks of the Vand Creek assemblage across an enigmatic contact that appears to have some structural modification but could still be stratigraphic (Figure 2). Overall, the foliation (S_T) found

FIGURE 4: Photographs of rocks representative of the Blanchard River assemblage. (a) Staurolite-bearing quartz-biotite schist with alternating quartz-rich and biotite-rich layers. Staurolite is found in more fine-grained biotite-rich layers and is replaced by cordierite and sillimanite (inset photo). (b) Example of graded bedding in quartz-biotite schist that is subvertical in orientation fining from right to left. (c) Intensely folded and dismembered migmatitic paragneiss of the KBgn unit. (d) Paragneiss of the Blanchard River assemblage (KBgn) near the contact with Ruby Range suite and Late Cretaceous diorite.

within the Blanchard River and Vand Creek assemblages in this area strikes northwest and dips moderately to the northeast. Unlike in the northeastern domain, F_T isoclinal folds are rarely observed in the southwestern domain. The L_T mineral lineations and crenulations in the Blanchard River assemblage are variable in the southwestern domain and plunge northwest to east-southeast. In the southernmost part of the study area, these L_T crenulations and fold hinges of the F_T isoclinal folds plunge moderately to the north-northeast. Leucosome within the paragneiss unit of the southwestern domain parallels the S_T fabric. Notably, the S_T foliation appears to be realigned parallel to the younger Tatshenshini shear zone in the southwestern domain. The intrusion of the Ruby Range suite postdates the development of D_T in the Blanchard River assemblage, crosscutting the S_T foliation.

3.2.2. D_{T+1}. D_{T+1} structures in the region are most prominent in the southwestern domain, defined by southeast-verging open folds (F_{T+1}; Figure 5(b)) that plunge moderately to the east-northeast and deform both S_0 and S_T. L_{T+1} lineations are primarily observed as crenulation lineations or by alignment of elongate minerals such as hornblende, aluminosilicates, and mica parallel to F_{T+1} fold hinges.

Few D_{T+1} structures were observed in the northeastern domain; however, in both outcrop and thin section, it is possible to see crenulations related to F_{T+1} folds deforming the S_T and S_0 fabrics. Additionally, pseudomorphed kyanite crystals are realigned parallel to the S_{T+1} axial surface (Figure 5(d)).

In the southwestern domain, large outcrop-scale F_{T+1} folds are visible (Figure 5(b)). L_{T+1} crenulation lineations and mineral lineations defined by the alignment of hornblende are oriented approximately parallel to F_{T+1} fold hinges, which plunge moderately to steeply towards the east-northeast. In addition to folding S_T, D_{T+1} also folds the leucosome within the pelitic paragneiss unit. The D_{T+1} deformation in the southwestern domain is more intense to the west and may be related to the Tatshenshini shear zone (Figure 2). The Ruby Range suite appears to be unaffected by the prominent D_{T+1} deformation throughout the field area.

3.3. Metamorphism. Herein metamorphic episodes assigned as M_{1C}, M_{2C}, and M_{3C} refer to Late Cretaceous to early Paleogene events that postdated deposition of the Blanchard River assemblage. We recognize one of the units in the study area also underwent Jurassic metamorphism (i.e., Yukon-Tanana terrane), which is inferred from the results of Clark

FIGURE 5: (a) Isoclinal folds (F_T) in the Blanchard River assemblage in the footwall of the Kluhini River thrust with S_0 bedding folded around the hinge. (b) Open F_{T+1} folding with vergence to the southeast observed in schist within the southernmost part of the study area. (c) Primary compositional bedding (S_0) of the Blanchard River assemblage parallel to S_T transposition fabric, with S_{T+1} observed x-cutting it. (d) Plane polarized light (PPL) photomicrograph of the rock observed in panel (c) where S_0 and S_T surfaces are visibly folded by F_{T+1}. Muscovite has pseudomorphed a porphyroblast (likely kyanite) and preserves inclusion patterns of S_T. Shear sense indicators within the S_T fabric indicate tops to the southwest sense of shear.

[44] ~130 km north of the study area; however, the Cretaceous-Cenozoic events in the current study area overprint this metamorphism.

Previous metamorphic analysis in the study area identified two recrystallization events [31] following the deposition of the Blanchard River assemblage. The first phase was related to a regional previously undated metamorphic event characterized by a high-pressure mineral assemblage of kyanite-staurolite-garnet-biotite-muscovite-ilmenite observed in the northeastern domain (sample 14-SI-088; also analyzed in this study; Figure 2) with peak pressure-temperature (P-T) conditions in the range of 635-650°C and 6.3-6.7 kbars [31]. The second event identified by Bordet et al. [31] is defined by a sillimanite and cordierite overprint in the southernmost parts of the field area that is associated with contact metamorphism and intrusion of the Ruby Range suite (64-51 Ma).

Detailed petrography from this study identified three metamorphic events that postdated deposition of the Blanchard River assemblage based on textural and fabric relationships of metamorphic minerals. The first phase of metamorphism (M_{1C}) is identified by amphibolite facies pressures and temperatures. This event is followed by M_{2C} that involved recrystallization during decompression. Finally, a third phase of metamorphism (M_{3C}) involved high-temperature, low-pressure contact metamorphism.

3.3.1. M_{1C} Burial. In both the Snowcap and Blanchard River, assemblages M_{1C} involved amphibolite facies metamorphism, characterized by porphyroblasts of kyanite and garnet within a quartz-biotite-plagioclase matrix (Figure 6). Staurolite porphyroblasts are included in this mineral assemblage, but only in rocks of the Blanchard River assemblage. Garnet porphyroblasts are <1 to 5 mm in diameter and have some quartz inclusions along fractured surfaces. Euhedral, unaltered garnet crystals are observed primarily in the northeastern domain and are best preserved within schist of the Snowcap assemblage (Figures 3 and 6). Biotite defining the penetrative S_T foliation in the study area is partly overgrown by, but also wraps around, garnet porphyroblasts, indicating that garnet grew syntectonically with respect to S_T (Figure 6). Poikioblastic kyanite and staurolite porphyroblasts 1-7 mm long contain inclusion trails of ilmenite, quartz, and biotite

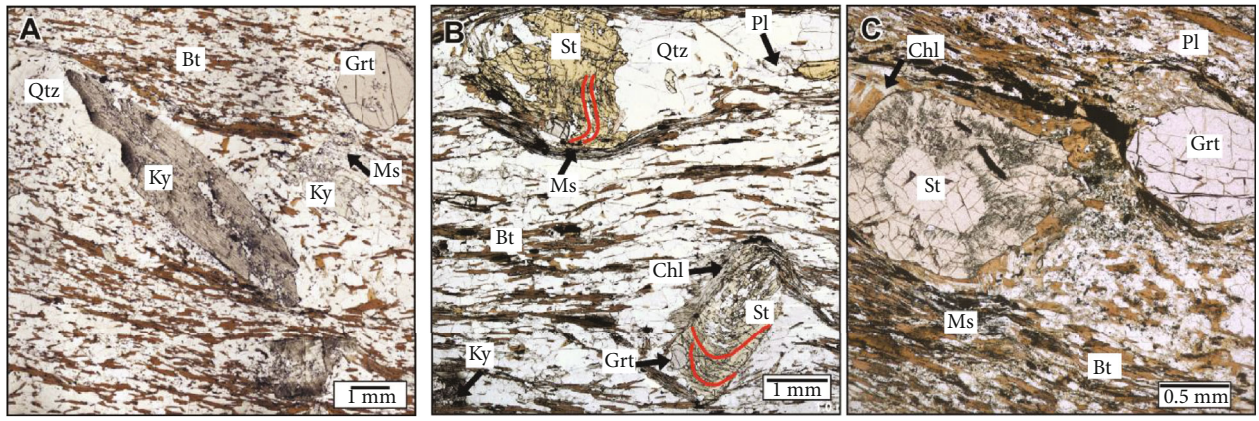

FIGURE 6: Defining features of M_{1C} prograde metamorphism. (a) PPL photomicrograph of Snowcap assemblage sample 16-LV-005 with prograde (M_{1C}) porphyroblasts of garnet and kyanite that have overgrown but are also wrapped by the S_T fabric. (b) PPL photomicrograph of Blanchard River assemblage sample 14-SI-088 garnet-kyanite-staurolite-biotite-quartz schist with some late chlorite and muscovite that is partially replacing garnet and staurolite. Sigmoidal inclusion trails in staurolite porphyroblasts are highlighted in red and align approximately parallel to the external S_T fabric along the outer edges of the porphyroblasts. (c) PPL photomicrograph of Blanchard River assemblage sample 16-LV-113 garnet-staurolite schist used for monazite petrochronology. M_{3C} chlorite and muscovite have partially replaced the prograde M_{1C} staurolite and garnet.

that have been rotated to align with the S_T foliation, which also wraps the porphyroblasts (Figure 6) suggesting syntectonic growth with respect to S_T. Although not recognized by Bordet et al. [31], the garnet-kyanite-staurolite mineral assemblage is also present in the southernmost area; however, most of the kyanite has been replaced by muscovite, cordierite, spinel, andalusite, and sillimanite (Figures 7 and 8).

3.3.2. M_{2C} Decompression. Locally, M_{1C} is overprinted by an M_{2C} assemblage characterized by the breakdown of garnet and kyanite, which we attribute to a period of decompression causing retrograde metamorphism. Evidence for M_{2C} retrogression includes the following: (1) spinel and plagioclase coronas surrounding relict kyanite porphyroblasts (Figure 7(a)); (2) garnet replaced by plagioclase and biotite (Figure 7(b)); and (3) kyanite is partly replaced by andalusite that appears to be in textural equilibrium with biotite (Figures 7(c) and 7(d)). Coronas surrounding garnet and kyanite porphyroblasts also include cordierite; however, the cordierite is commonly accompanied by sillimanite, which is part of a later high-temperature metamorphic overprint (discussed in M_{3C} below). Andalusite porphyroblasts appear to have underwent deformation as they exhibit undulose extinction, as well as grain boundary migration textures (Figure 8(a)), which indicates that D_{T+1} deformation persisted during and after M_{2C}.

3.3.3. M_{3C} Contact Metamorphism. M_{3C} is characterized by high-temperature, low-pressure static recrystallization of sillimanite and cordierite that overprint M_{1C} and M_{2C}, as well as D_T and D_{T+1} fabrics (Figure 8). Sillimanite pseudomorphs that statically replace kyanite porphyroblasts are most common throughout the southwestern domain of the study area, particularly within the paragneiss (Figures 8(b) and 8(c)). The static recrystallization of M_{3C} minerals such as cordierite, sillimanite, and mimectically recrystallized biotite that overprint D_{T+1} crenulations indicate the D_{T+1} deformation ended prior to this high-temperature event. Growth of M_{3C} sillimanite is directly correlated with distance from the Ruby Range suite, with a greater abundance of M_{3C} sillimanite observed closer to the Paleocene to Eocene intrusive suite. Although M_{3C} is best preserved in the southwestern domain, overprinting relationships of M_{1C} by M_{3C} are also observed in the northern parts of the study area where prograde minerals such as kyanite, staurolite, and garnet are replaced by muscovite, chlorite, and trace amounts of cordierite within M_{1C} pressure shadows (Figure 6), or as muscovite pseudomorphs of earlier porphyroblasts (likely kyanite; Figure 5(d)).

4. Monazite Geochronology

4.1. Methods. Twelve representative metapelitic and metapsammitic samples from the study area (Figure 2(a)) were selected for Quantitative Evaluation of Materials by Scanning Electron Microscopy (QEMSCAN) at SGS Canada labs in Burnaby, BC, to create mineral maps for thin sections. These maps were used to determine the abundance, size, and locations of all monazite and zircon crystals in each thin section. All samples were analyzed with the Field Image technique described by Pirrie [60] using a 20 μm step interval over a 20 mm x 30 mm area. System configurations were set to run at 20 kV with a measured beam current of 10 nA, which was monitored and adjusted throughout the analyses. The search routine for finding monazite and zircon crystals was done using a sparse mineral search mode (SMS) set to 95 while the section was scanned at 5 μm resolution using backscatter electron (BSE) only. Frames containing bright phases were then analyzed using X-ray signal at 5 μm resolution with the frame size minimized to 500 μm across to map the area surrounding a mineral of interest. Eight thin sections, containing up to 30 monazite crystals that were ≥17 μm

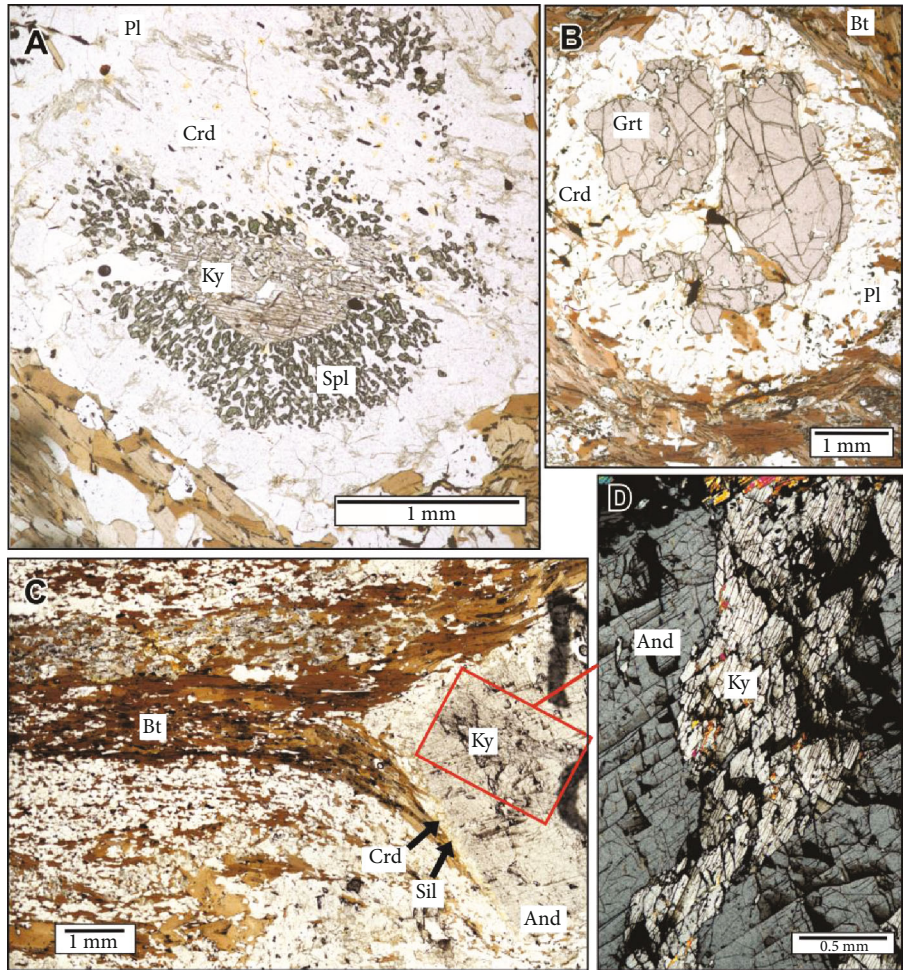

FIGURE 7: Defining characteristics of M_{2C} metamorphism related to decompression and cooling. (a) PPL photomicrograph of kyanite in sample 16-LV-170 surrounded by a corona of spinel, cordierite, and plagioclase. (b) PPL photomicrograph of garnet in sample 16-LV-164 partially replaced by a corona of cordierite, plagioclase, and biotite. (c, d) Photomicrographs of sample 16-LV-294 paragneiss where andalusite in equilibrium with biotite has overprinted kyanite shown in PPL (c) and crossed polarized light (d).

along their short axis (preferably ≥20 μm) and in texturally meaningful locations within each sample, were selected for compositional mapping.

Compositional mapping for monazite was carried out using the Cameca SX100-Ultrachron at the University of Massachusetts. Maps were collected for Y, Ca, Th, U, and Nd using Y Lα (TAP monochromator), Ca Kα (LPET), Th Mα (LPET), U Mβ (VLPET), and Nd Lα (LLIF). Collection conditions were run at 15 kV, 300 nA, with a focused beam with 40 ms per pixel dwell times. The location of spots for U-Pb in situ geochronology were selected based on chemical zoning of Y in monazite maps (Figure 9, Supplementary 2(A–H)), which has been shown to correlate with episodes of growth and breakdown of garnet [61–64].

Monazite crystals were analyzed for U-Th-Pb geochronology and trace element geochemistry using Laser Ablation Split Stream Inductively Coupled Plasma Mass Spectrometry (LASS-ICP-MS) (Figure 9; Supplementary 2(A–H); Supplementary 3) at the University of California Santa Barbara (UCSB), which facilitated simultaneous isotopic and elemental analysis from a single spot [65]. Dates were calculated following the procedures of Stern and Berman [66] and Ireland and Gibson [67], using the $^{206}Pb/^{238}U$ decay system corrected for common Pb using the ^{207}Pb correction. For this study, the $^{206}Pb/^{238}U$ date is preferred because it is the most precise U-Pb chronometer for relatively young monazite that typically have low ^{207}Pb values, and there was no noticeable reverse discordance that would indicate issues arising from excess ^{206}Pb due to ^{230}Th disequilibrium [68, 69]. Although the $^{208}Pb/^{232}Th$ chronometer would be ideal to use, given the relatively high concentration of these isotopes in monazite and being unaffected by the ^{230}Th disequilibrium problem, there are few accepted values for $^{208}Pb/^{232}Th$ ages of reference materials. Nonetheless, the $^{206}Pb/^{238}U$ dates were generally within error of the $^{208}Pb/^{232}Th$ dates. We do not consider monazite dates to have been reset by thermally activated diffusive Pb loss, as peak temperature estimates for these samples are 635-650°C [31]. For noticeable diffusive Pb loss to occur, monazite crystals of the size that were analyzed (typically ~20-50 μm along its shortest axis; Supplementary 2(A–H)) would have to be exposed to temperatures >800°C for an unrealistic length of geological time based on

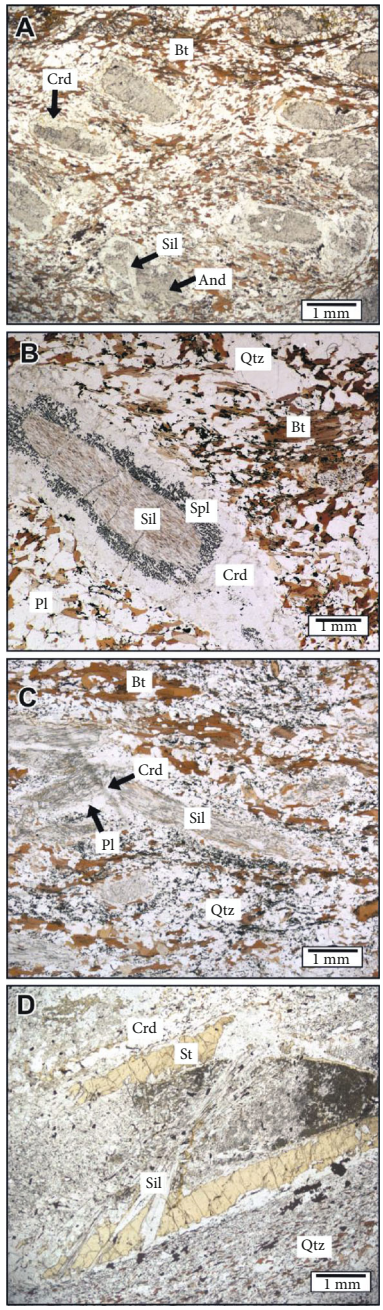

FIGURE 8: Defining characteristics of M_{3C} metamorphism. (a) PPL photomicrograph of sample 16-LV-248 paragneiss where andalusite is replaced by cordierite and sillimanite. Biotite aggregates within this sample do not show evidence of deformation (e.g., relatively equant shape, lack of mechanical twinning, and uniform extinction) but are found to have mimectically recrystallized about F_{T+1} folds. (b) PPL photomicrograph for sample 16-LV-170 thin section used for monazite petrochronology where kyanite has been completely pseudomorphed by sillimanite within the cordierite, spinel, and plagioclase corona. (c) PPL photomicrograph for sample 16-LV-211 used for monazite petrochronology where sillimanite, cordierite, and plagioclase have completely pseudomorphed an unknown porphyroblast (possibly kyanite or staurolite). (d) PPL photomicrograph of sample 16-LV-208 with staurolite overprinted by sillimanite, cordierite, and plagioclase.

parameters determined experimentally by Cherniak et al. [70] and Gardes et al. [71].

In the analyses, a correlation can be made between low concordance percentage and low *P* values indicating something other than monazite was included in the spot analysis (e.g., inclusion and penetration into the epoxy); this was used as an additional filter for data to be rejected. When comparing spot locations from the laser to the monazite maps, there are some spots that may have overlapped compositional zones, such as high and low Y zones. As these spots may represent mixed dates, they typically were not considered in the determination of final ages. Best ages for each monazite spot were calculated using the ^{207}Pb-corrected ratio of ^{238}U/^{206}Pb in Tera-Wasserburg plots (Figure 10) following procedures described by Ireland and Gibson [67]. Furthermore, using these "best ages," weighted mean ages were calculated for groups of analyses within a given thin section that targeted specific chemical domains with similar dates and textural settings in the monazite crystals, such as low Y cores or high Y rims (Table 1). Additional to Y zonation, distribution patterns of heavy rare earth elements (HREE) were also considered when distinguishing the different age domains.

4.2. Results. The U-Th-Pb and select trace element data used in the age determinations are provided in the Supplementary 3(A); additional trace element results are reported in Supplementary 3(B). A summary of monazite petrochronology ages is provided in Table 1. Complete thin section images showing all locations of the monazite analyzed for each sample, accompanied by Y maps for each monazite with spot locations are provided in Supplementary 2(A–H).

4.2.1. Yukon-Tanana Terrane, Snowcap Assemblage

(1) Sample 16-LV-005. This sample is from a fine- to medium-grained garnet-kyanite schist with a matrix of quartz, biotite, and plagioclase. Less abundant late muscovite and chlorite is found in pressure shadows surrounding porphyroblasts of kyanite and garnet, as well as locally in the matrix. Elongate monazite crystals are aligned parallel to the foliation in the matrix, around the edges of biotite crystals and within pressure shadows of kyanite and garnet porphyroblasts. Although some crystals occur as inclusions within kyanite porphyroblasts (e.g., monazite 15; Figure 9), they are generally located along fracture surfaces. Thus, they may not record monazite growth preceding incorporation into the porphyroblast and could relate to later growth within the fractures. The dates of the 16 monazite crystals analyzed for this sample range from ca. 76 to 65 Ma within 26 spots (Supplementary 3(A)). A weighted mean age of 70.3 ± 0.5 Ma with a mean squared weighted deviate (MSWD) of 1.9 was calculated excluding two outlying dates of 75.9 and 65.4 Ma (Figure 10(a)). Monazite dates used to determine the weighted mean age were in a variety of textural locations such as within the matrix, inclusions, and pressure shadows surrounding porphyroblasts. In many of the monazite crystals, Y domains were too irregular or too small to target, and there does not appear to be an obvious correlation between Y content and date. Relatively small monazite

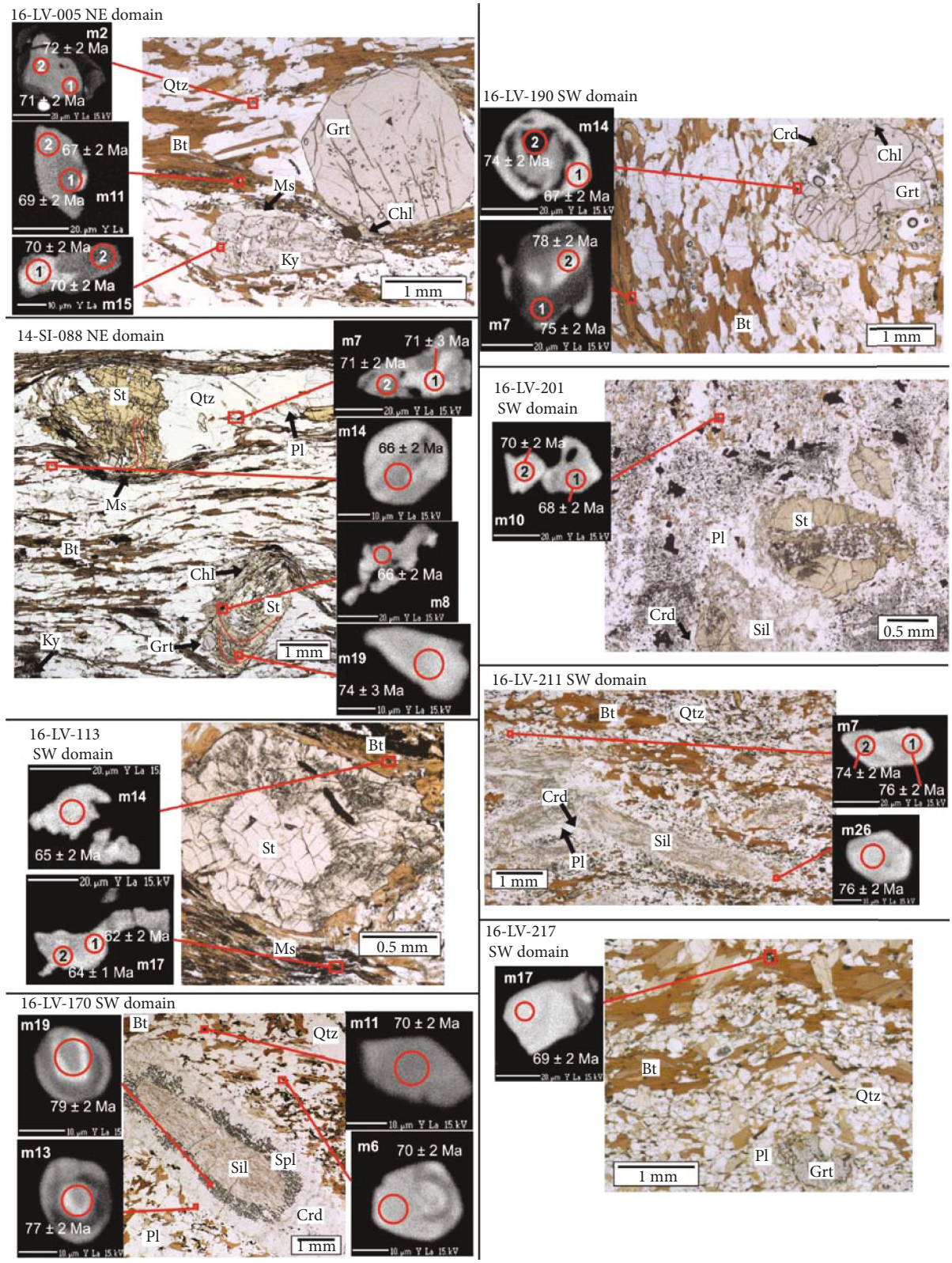

FIGURE 9: PPL photomicrographs of samples showing mineral assemblages of respective samples and textural locations of monazite crystals analyzed by in situ LASS-ICPMS. Individual monazite maps show zonation of Y within monazite crystals and the locations of the spot analyses with their corresponding dates. Note that the Y map brightness and color are not the same scale from crystal to crystal.

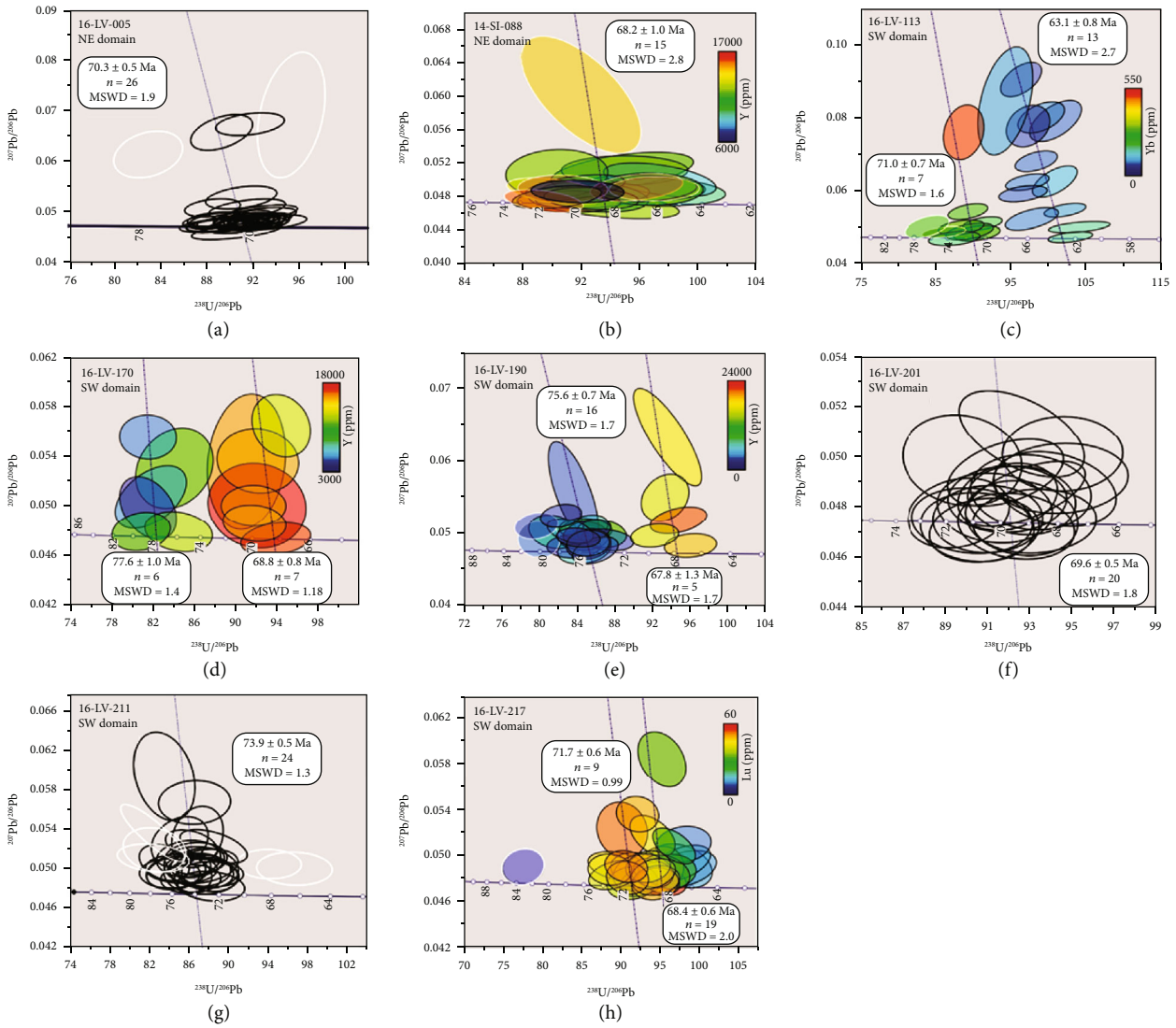

Figure 10: Tera-Wasserburg diagrams showing U-Pb isotope data for samples analyzed by in situ LASS-ICPMS. Regression lines are anchored on the initial $^{207}Pb/^{206}Pb$ ratio determined using the Stacey and Kramers [72] two-stage Pb evolution curve and the weighted mean age. Graphs with color gradients show the relative abundance of trace elements (either Y, Yb, or Lu) used to help differentiate age domains. Data outliers are outlined in white; calculated weighted mean ages are provided in white boxes.

Table 1: Summary of monazite petrochronology results.

Domain	Sample	TE	Weighted mean ages (Ma)		Outlying dates (Ma)
			High TE	Low TE	
NE	16-LV-005	n/a	70.3 ± 0.5; MSWD 1.9		75.9, 65.4
NE	14-SI-088	Y	68.2 ± 1.0; MSWD 2.8		
SW	16-LV-113	Yb	71.0 ± 0.7; MSWD 1.6	63.1 ± 0.8; MSWD 2.7	76.2, 74.3
SW	16-LV-170	Y	68.8 ± 0.8; MSWD 1.18	77.6 ± 1.0; MSWD 1.4	
SW	16-LV-190	Y	67.8 ± 1.3; MSWD 1.7	75.6 ± 0.6; MSWD 1.7	80.0
SW	16-LV-201	n/a	69.6 ± 0.5; MSWD 1.8		
SW	16-LV-211	n/a	73.9 ± 0.5; MSWD 1.3		77.4, 66.1, 67.9
SW	16-LV-217	Lu	71.7 ± 0.6; MSWD 0.99	68.4 ± 0.6; MSWD 2.0	82.9

NE: northeast; SW: southwest; TE: trace element used to correlate dates in specific chemical domains in order to differentiate age domains.

crystals generally contained moderate to high Y values and produced the youngest dates 70 Ma or less (e.g., monazite 05 and 15; Supplementary 3(A); Supplementary 2(A)).

4.2.2. Blanchard River Assemblage

(1) Sample 14-SI-088. This sample is from the immediate footwall of the Kluhini River thrust in the northeastern domain (Figure 2). It is a kyanite-staurolite-garnet schist with a matrix of quartz, biotite, plagioclase, and muscovite. Twenty-eight spots in nineteen monazite crystals were analyzed, which produced a seemingly continuous spread of monazite dates from 74 to 64 Ma. In the trace element data (Supplementary 3(A)), it was observed that monazite crystals with >14000 ppm of Y had the greatest spread of dates. Monazite crystals with <14000 ppm of Y had a more restricted range of dates and were used to calculate a weighted mean age of 68.2 ± 1.0 Ma (MSWD = 2.8) (Figure 10(b)). Although this MSWD value is slightly higher compared to other samples, the weighted mean age of ca. 68 Ma is consistent with weighted mean ages from other Blanchard River assemblage samples (discussed below).

Within this sample, monazite crystals are generally elongate parallel to the foliation, particularly crystals with dates of ca. 70 Ma. Overall, there is no significant Y zonation within the monazite crystals, which all return similar dates. It is notable that the youngest monazite crystals are in proximity to muscovite that grew at the expense of M_{1C} porphyroblasts (e.g., monazite 8; Figure 9). The monazite crystal with the oldest date of ca. 74 Ma (monazite 19; Figure 9; Supplementary 2(B)) is found included in a staurolite porphyroblast.

(2) Sample 16-LV-113. This sample is a staurolite-garnet schist with a matrix of biotite, quartz, and plagioclase. Trace amounts of muscovite and chlorite partially replace staurolite and garnet within pressure shadows (Figure 9). Twenty-one monazite crystals were analyzed, and 20 spot analyses are used. Monazite dates in this sample range from 76 to 61 Ma, the largest range of dates of all samples. There is a correlation between monazite dates and relative proportions of HREE, particularly Yb, with the older dates correlating to higher ppm of HREE and young dates correlating to a relative depletion in HREE (Figure 10(c)). The resulting weighted mean from the high Yb monazite crystals is 71.0 ± 0.7 Ma with an MSWD of 1.6. The low Yb monazite crystals resulted in a weighted mean of 63.1 ± 0.8 Ma with an MSWD of 2.7.

Notably, the oldest monazite crystal with dates of 76 and 74 Ma is found within a pressure shadow of relict staurolite. This elongate monazite crystal did not grow parallel to the biotite grain encasing it, suggesting that this crystal had grown prior to biotite crystallization. Monazite crystals with dates of ca. 70 Ma are found primarily within the matrix or along the edge of biotite grains. Monazite crystals with dates around 63-61 Ma are consistently found either texturally associated with muscovite that has grown in pressure shadows surrounding staurolite and garnet porphyroblasts or parallel to the grain boundaries of matrix muscovite, similar to textural relationships observed in sample 14-SI-088.

(3) Sample 16-LV-170. This sample is a kyanite-garnet-cordierite-sillimanite paragneiss with a matrix of quartz, plagioclase, biotite, and cordierite. Relict kyanite crystals in this sample are found encased in coronas of plagioclase, spinel, and cordierite; some of these kyanite crystals have also been completely pseudomorphed by sillimanite (Figures 7(a), 8(b), and 9). Eighteen monazite crystals were analyzed with a total of 22 laser spots. Thirteen of these spots were deemed free of date mixing. There is a correlation between Y concentration in the analyzed monazite crystals and date defining a bimodal distribution in this sample. When plotting the date against Y concentration (Figure 10(d)), older dates correlate to relatively Y poor (dark) zones or crystals (with the exception of one spot), whereas younger dates correlate to relatively Y rich (light) zones or crystals. The respective weighted mean ages are 77.6 ± 1.0 Ma (MSWD = 1.4) in Y poor zones and 68.8 ± 0.8 Ma (MSWD = 1.18) in Y rich zones.

Texturally, monazite crystals with lower Y content are found in coronas of relict M_{1C} porphyroblasts or within foliation-defining biotite grains, suggesting that they were inclusions within M_{1C} minerals such as kyanite prior to their replacement. Thus, the oldest dated monazite crystals appear to have crystalized prior to or during the first phase of metamorphism (M_{1C}) recognized in the Blanchard River assemblage. Monazite crystals rich in Y are commonly located within or around biotite or along cracks of M_{1C} porphyroblasts, suggesting that the younger monazite crystallized during the breakdown of M_{1C} metamorphic minerals during M_{2C}.

(4) Sample 16-LV-190. This sample is a garnet-sillimanite-cordierite schist with a matrix of quartz and plagioclase. Petrography shows that garnet is partly replaced by sillimanite and cordierite, and trace amounts of muscovite and chlorite replace M_{1C} minerals (Figure 9). Twenty monazite crystals were analyzed, and 21 spots were selected for age analysis. There is a correlation between Y content and date, with relatively Y poor domains corresponding to older monazite dates and relatively Y rich domains to younger monazite (Figure 10(e)). The respective weighted mean ages of these domains are 75.6 ± 0.6 Ma (MSWD = 1.7) and 67.8 ± 1.3 Ma (MSWD = 1.7), with two outlying dates of 80 ± 2 Ma. The two outlying dates of 80 Ma are within low Y zones in the cores of monazite grains, which likely indicates preservation of an earlier phase of monazite crystallization during prograde metamorphism. Several of the monazite crystals that have obvious zoning of high and low Y, such as monazite 14, are found in proximity to relict garnet porphyroblasts (Figure 9; Supplementary 2(E)). Texturally, young monazite crystals are found in contact with the edge of matrix biotite grains. Many elongate monazite crystals are oriented parallel to the foliation, defined by the alignment of biotite, and some of these elongate crystals are completely encased by biotite, which means that they could have grown during M_{2C} metamorphism involving the breakdown of the prograde metamorphic assemblage.

(5) Sample 16-LV-201. This sample is a fine-grained staurolite-garnet schist with a matrix of biotite, plagioclase, quartz, and trace amounts of pyrite throughout (Figure 9). Within the 21 monazite crystals analyzed, 20 were deemed free of mixing. Monazite crystals within this sample have relatively high Y content compared to previous samples but are generally not zoned in Y. The dates range from 72-67 Ma and result in a weighted mean of 69.6 ± 0.5 Ma (MSWD = 1.8) (Figure 10(f)). Texturally, these monazite crystals are found primarily within the matrix where they are aligned parallel to the foliation (Figure 9).

(6) Sample 16-LV-211. This sample is a sillimanite-bearing paragneiss with a matrix of quartz, biotite, plagioclase, and cordierite (Figure 9). Thirty-three spots were analyzed on 28 monazite crystals; 29 of these spots were chosen for analysis. U-Pb dates in this sample range from 77 to 66 Ma. A weighted mean age of 73.9 ± 0.5 Ma (MSWD = 1.3) was calculated excluding outlying spots of 77 Ma, 66 Ma, and 68 Ma because they are noticeably older and younger, respectively, than the rest of the analyses (Figure 10(g)).

Overall, monazite crystals are moderately high in Y with mottled zonation, making it difficult to identify spots that may have overlapped more than one trace element domain. Monazite crystals that have the oldest dates between 77 and 75 Ma are found texturally surrounding the sillimanite pseudomorphs of elongate minerals (likely kyanite) and relict staurolite porphyroblasts. The only monazite crystal that has a low Y zone resulted in a date of ca. 75 Ma, consistent with older ages observed in previous samples. In contrast, the monazite crystals that have dates of ca. 70 Ma are found in the matrix surrounded by quartz or plagioclase.

(7) Sample 16-LV-217. This sample is a medium-grained garnet-bearing paragneiss with a matrix of quartz, plagioclase, and biotite (Figure 9). Of the thirty-five spots analyzed in twenty-four monazite crystals, only one spot was rejected. Dates from this sample range from 73 to 65 Ma, with one outlying date of 83 Ma. A weighted mean age excluding the one outlier is 69.3 ± 0.7 Ma with an MSWD of 4.4 indicating an excess amount of scatter. Yttrium maps display primarily unzoned monazite with moderately high Y relative to other samples. Although Y values appear to be relatively consistent, there is a notable correlation between HREE such as Yb and Lu and date. Calculating the average age of monazite based on relatively low and high Lu content significantly improved the MSWD values, resulting in ages that are, respectively, 71.7 ± 0.6 Ma (MSWD of 0.99) and 68.4 ± 0.6 Ma (MSWD of 2.0) (Figure 10(h)). Monazite 11 (Supplementary 2(H)) is the only zoned crystal with a low Y core and high Y rim providing dates of 83 ± 2 Ma and 70 ± 2 Ma, respectively.

Monazite crystals in this sample are found in contact with or encased in biotite that has been mimectically recrystallized by a younger generation of biotite parallel to the S_T foliation. Overall, monazite crystals with dates of ca. 71 Ma have grown within these recrystallized biotite grains (monazite 13), and younger dates of ca. 68 Ma grew more towards the edge of biotite grains (monazite 27; Supplementary 2(H)). The youngest monazite crystal with a date of ca. 65 Ma overgrew seemingly undeformed biotite indicating that its growth postdated the recrystallization of the biotite. The single monazite grain (monazite 11) that has a date of ca. 83 Ma is oriented parallel to the S_T foliation, which indicates growth occurred pre- to syn-S_T. Besides monazite 11, most of the elongate monazite crystals in this section are not obviously aligned with the foliation, suggesting growth occurred after the formation of the foliation.

5. Discussion

5.1. Late Cretaceous to Paleocene Tectonometamorphic Evolution of the Blanchard River Assemblage. Metamorphic, structural, and petrochronological results from this study provide important new information to reconstruct the tectonometamorphic evolution for the Blanchard River assemblage, and by corollary new timing constraints related to metamorphism associated with terminal accretion of the Insular terranes in southwest Yukon. Notably, following ca. 126 Ma deposition of the Blanchard River assemblage and up to the Paleogene intrusion of the Ruby Range suite (64-51 Ma), there are at least three distinct tectonic events that affected the region including (1) overthrusting of Yukon-Tanana terrane resulting in tectonic thickening and amphibolite facies metamorphism (M_{1C}-D_T), (2) decompression resulting in the growth of M_{2C} minerals, followed by D_{T+1} deformation, and (3) intrusion of the Ruby Range suite resulting in the replacement of previous metamorphic mineral assemblage with high-temperature, low-pressure M_{3C} minerals. The following provides a detailed overview of timing constraints for the tectonic events summarized above based on the results of this study.

5.1.1. M_{1C}-D_T Compression. The first phase of deformation (D_T) and development of the northwest-striking transposition foliation (S_T) that is associated with regional amphibolite facies metamorphism (M_{1C}) is congruent with the southwest-directed Kluhini River thrust placing the Yukon-Tanana terrane over the Blanchard River assemblage. Bordet et al. [31] calculated P-T conditions of the prograde assemblage consisting of garnet, kyanite, staurolite, biotite, muscovite, and ilmenite from sample 14-SI-088 in the northeastern domain to be between 635-650°C and 6.3-6.7 kbars, which equates to ~25 km depth assuming a crustal density of ~2800 kg/m^3. We infer that these peak amphibolite facies conditions were also attained in the southernmost part of the study area as relict kyanite is present and incompletely replaced by retrograde andalusite, spinel, and plagioclase (Figure 7). This incomplete replacement indicates that andalusite did not grow with the prograde assemblage, contrary to what was originally proposed by Bordet et al. [31]. Furthermore, the low-pressure estimation of ~3.5-4 kbar for the growth of andalusite and staurolite in the southwestern domain attributed to prograde metamorphism [31] does not reflect pressure conditions attained in the area as staurolite and andalusite did not grow in equilibrium with one another.

Ages from relatively Y poor domains in monazite crystals are between 83 Ma and 76 Ma and are most often located texturally within and surrounding relict M_{1C} porphyroblasts or included in foliation-forming matrix biotite. This correlation between Y concentration and age is consistent with previous studies, which have indicated that the production and consumption of monazite is sensitive to Y content available within the effective bulk rock composition [61–64]. These studies concluded that low Y zones in monazite can be explained by growth during or after garnet crystallization due to the preferential fractionation of Y into garnet during its growth, which substantially reduces the Y available in the effective bulk rock reservoir for uptake into monazite forming at that time [61–64]. Applying these principles to the Blanchard River assemblage, garnet growth is interpreted to have occurred during prograde metamorphism along with kyanite and staurolite, indicating that ages of 83-76 Ma from Y-poor monazite zones constrain the timing of prograde amphibolite facies metamorphism. The textural relationships between prograde metamorphic minerals such as kyanite and staurolite and the S_T fabric indicate syntectonic M_{1C} porphyroblast growth in both the Blanchard River assemblage and the Yukon-Tanana terrane.

The interstitial leucosome found primarily within the paragneiss unit in the southwestern domain both parallels and crosscuts D_T structures, indicating that leucosome generation would have occurred late syn- to post-D_T deformation, which best correlates to the timing of the intrusion of the Late Cretaceous orthogneiss (78-76 Ma) [30]. Crosscutting relationships of the Ruby Range suite over paragneissic fabrics indicate that the intrusion of the Ruby Range suite is not responsible for this partial melting.

It is notable that the metamorphic assemblage and age of peak metamorphism in the Yukon-Tanana terrane sample is apparently the same as that in the Blanchard River assemblage. Other than an older fabric that has been refolded by the D_T event, there is limited evidence of Jurassic tectonism in the Yukon-Tanana terrane rocks within the area. There is also an absence of Jurassic monazite in the Yukon-Tanana terrane sample (16-LV-005), which may suggest the Jurassic metamorphic assemblage associated with the older fabric in the Yukon-Tanana terrane thrust sheet did not achieve P-T conditions favorable for monazite growth, and/or the Cretaceous overprint of M_{1C} was so pervasive that it completely recrystallized the metamorphic assemblage (and any Jurassic monazite within it).

5.1.2. M_{2C}-D_{T+1}. A second phase of metamorphism is interpreted to have occurred at ca. 70 Ma with the breakdown of the prograde metamorphic assemblage. High Y monazite with ages of ca. 70 Ma are most commonly found within the matrix and in pressure shadows around M_{1C} porphyroblasts. The production of high Y monazite is interpreted to be the product of M_{1C} garnet breakdown that would have released Y into the effective bulk rock composition from which the monazite crystallized [62–64]. Petrologic evidence for garnet breakdown is the replacement of garnet by plagioclase, biotite, and quartz (Figure 7). Additional M_{1C} breakdown is expressed in the southernmost part of the area where kyanite is replaced by andalusite (Figures 7(c) and 7(d)). A decompression reaction between kyanite with the matrix is also expressed by coronas of spinel, plagioclase, and cordierite surrounding kyanite (Figure 7). Plagioclase and spinel coronas surrounding kyanite are a feature commonly related to decompression from high P metamorphic facies; however, this texture is not considered to be indicative of a particular P-T condition [73, 74]. Within the southernmost part of the field area, a critical textural relationship to estimate pressure conditions and timing for the M_{2C} event was observed. This texture is biotite that crystalized in equilibrium with andalusite (Figures 7(c) and 7(d)) and is texturally associated with ca. 70 Ma monazite crystals. Equilibrium conditions of coexisting biotite and andalusite in pelitic rocks is interpreted to occur below 3 kbar [75], suggesting that the rocks of the Blanchard River assemblage underwent at least 3.3 kbar of decompression (at least 10-15 km) by ca. 70 Ma, which equates to an exhumation rate of ~1-1.5 km/Myr. This breakdown of kyanite, first into andalusite and not sillimanite, would indicate that the decompression would have to be accompanied by cooling [75]. Although extensional faults that could have facilitated tectonic denudation of ~10-15 km of crust at an exhumation rate of ~1-1.5 km/Ma were not identified in the study area, this could be attributed to enhanced erosional processes within an uplifting orogen [76].

The second deformational event (D_{T+1}) that is observed throughout the field area is based on the folding of S_T and S_0 by southeast-verging undulating open folds (F_{T+1}). Undulose extinction in M_{2C} andalusite indicates that it has been deformed during or after its crystallization (Figure 8(a)), constraining D_{T+1} deformation to have occurred during or after the ca. 70 Ma M_{2C} metamorphism. Textures depicting the D_{T+1} deformation in combination with high Y monazite relating to prograde assemblage breakdown were critical when deciphering the presence of M_2 metamorphism in the study area, without which an alternate metamorphic interpretation could have been made. This alternate interpretation would involve exhumation with little to no petrographic expression before a progressive reheating at a low pressure, resulting in the growth of mineral assemblages including andalusite and sillimanite. Although this interpretation can explain the metamorphic assemblages observed, it does not fully account for the other deformational, textural, and petrochronological lines of evidence that have been collected.

D_{T+1} structures are predominantly observed in the southwestern domain of the field area; however, it is unclear whether this deformation has any correlation to the Tatshenshini shear zone. In the southwestern domain, the S_T foliation strikes parallel to the Tatshenshini shear zone and dips moderately to the east-northeast, in contrast with the north-dipping S_T fabric in the northeastern field areas paralleling the Kluhini River thrust (Figure 2 and Supplementary 1). This suggests that there could have been a realignment of the S_T foliation in the southwestern domain related to movement along the Tatshenshini shear zone. Alternatively, the shear zone could have an older tectonic history related to D_T deformation (e.g., [59]) and has since been reactivated. Although it is not clear how deformation along the Tatshenshini shear zone affected the Blanchard River assemblage and

the underlying Vand Creek assemblage, there is clear deformation in the Ruby Range suite within the immediate hanging wall of the Tatshenshini shear zone. Foliations within this part of the Ruby Range suite strike parallel to the shear zone with mineral lineations that plunge moderately to the east-northeast (Supplementary 1). These observations suggest that deformation related to the Tatshenshini shear zone occurred during or after the intrusion of the earliest phases of the Ruby Range suite (ca. 64 Ma), as younger phases of the intrusive suite are massive and do not reflect this deformation [30, 57].

5.1.3. M_{3C}. M_{3C} contact metamorphism is attributed to the intrusion of the Ruby Range suite and is most prevalent in the southernmost part of the study area where there is significant static overprinting of M_{1C} and M_{2C} assemblages by sillimanite and cordierite (Figure 8). The static overprint of cordierite and sillimanite, as well as mimectic recrystallization of biotite that overprints D_{T+1} crenulations observed in thin section, indicates M_{3C} postdates D_{T+1} deformation. The youngest population of monazite observed in the study area is texturally associated with muscovite, and to a lesser degree chlorite that grew by replacement of staurolite, kyanite, and garnet, which is interpreted to be the result of heating (Figures 5 and 6). These monazite crystals can have relatively low HREE content, which is likely due to a lack of availability of these trace elements during this phase of mineral growth. The monazite crystals associated with the breakdown of staurolite into muscovite give ages between ca. 63 and 61 Ma, which is coeval with the older portions of the Ruby Range suite documented in southwest Yukon (64-51 Ma) [9, 30, 31, 57].

5.2. Implications for Late Cretaceous to Paleocene Tectonism in Southwest Yukon and the Northern Cordillera. Jurassic-Cretaceous-aged overlap assemblages along with Coast Mountains arc related intrusions situated between the Intermontane and Insular terranes (Figure 1) provide evidence for contractional tectonism related to accretion of the Insular terranes. The following compares the tectonic events recorded in the Blanchard River assemblage to similar assemblages and tectonic settings within southwest Yukon and throughout the Canadian and Alaskan Cordillera to provide new insight into the history of the Insular-Intermontane suture zone.

5.2.1. Southwest Yukon. The Late Cretaceous tectonometamorphism documented in the Blanchard River assemblage has many similarities to that recorded in the Kluane schist located immediately to the north and northwest of the study area (Figure 1). In the Kluane schist, ca. 82 Ma metamorphic rims on detrital zircon record the overthrusting of the Yukon-Tanana terrane [30, 34]. This is consistent with the 83-76 Ma ages attributed to tectonic thickening in the Blanchard River assemblage. Peak amphibolite facies conditions within the Blanchard River assemblage are also consistent with those calculated for the Kluane schist, which are ~7 kbar and 500°C [34]. Within the study area, 78-76 Ma orthogneiss was deformed syntectonically with the Blanchard River assemblage; similar orthogneiss bodies have also been observed within the Kluane schist [30]. These correlations, along with corresponding structural relationships with the Yukon-Tanana terrane, suggest that there was a widespread tectonometamorphic event that affected both the Blanchard River assemblage and the Kluane schist in southwest Yukon. This event is interpreted to reflect the southwestward-directed thrusting of Yukon-Tanana terrane rocks overtop of these basinal assemblages in response to the Late Cretaceous collapse of the basins [9, 30, 77], leading to the terminal accretion of the Insular terranes onto the northwestern Laurentian margin.

Following the compression and tectonic burial of these Jura-Cretaceous basins, there is evidence of exhumation to upper crustal levels accompanied by cooling in both Blanchard River assemblage and the Kluane schist at ca. 70 Ma. Israel et al. [30] recorded ca. 70 Ma metamorphic rims on detrital zircon in the Kluane schist, as well as ca. 70 Ma syn- to posttectonic dikes. Ages of these zircon and dikes can be directly correlated to monazite ages related to decompression of the Blanchard River assemblage and growth of the low-temperature M_{2C} metamorphic assemblage. Similar to the ~10-15 km of exhumation in the Blanchard River assemblage, the Kluane schist is also interpreted to have undergone 9-12 km of exhumation postregional metamorphism, and prior to the intrusion of the Ruby Range suite [34]. The youngest monazite ages in the Blanchard River assemblage at ca. 63-61 Ma are somewhat older than those observed in the Kluane schist (57-55 Ma); however, both ages are within the time span of the intrusion of the Ruby Range suite [30, 34, 35, 57, 78]. Within the Kluane schist, Mezger et al. [34] identified a contact aureole 5-6 km wide with staurolite, andalusite, and cordierite restricted to high-grade parts of the aureole. Similarly, contact metamorphism responsible for the growth of cordierite and sillimanite in the Blanchard River assemblage is interpreted to be related to the intrusion of the Ruby Range suite. In contrast with the Kluane Schist, we only observe intense overprinting of the M_{1C} and M_{2C} assemblages directly adjacent to the contacts with the Ruby Range suite as opposed to a 5-6 km wide aureole.

5.2.2. Comparison with Western Canadian and Alaskan Cordillera. Jura-Cretaceous basinal sequences similar to the Blanchard River assemblage and the Kluane schist are juxtaposed between the Insular and Intermontane terranes along the length of the BC-Yukon-Alaska Cordillera (Figures 1 and 11) [12, 14]. From west-central BC into southern Alaska, there is evidence of Late Cretaceous crustal thickening in a compressional environment, marking the collapse of these Jura-Cretaceous basins [12, 14, 28, 79]. This crustal thickening is attributed to west-vergent thrusting of the Intermontane terranes against the Insular terranes [15, 19, 21] and has been linked to widespread compression across the Coast Mountains orogen [19, 80, 81]. The 83-76 Ma tectonism in southwest Yukon is broadly consistent with Late Cretaceous deformation and metamorphism observed along the length of the western Canadian-Alaskan Cordillera; however, there are examples where deformation occurred up to 10 Myr later in southwest Yukon than in west-central BC (Figure 11). For instance, in the southwestern Coast Mountains, there is a system of west-vergent reverse faults related to the oldest tightly

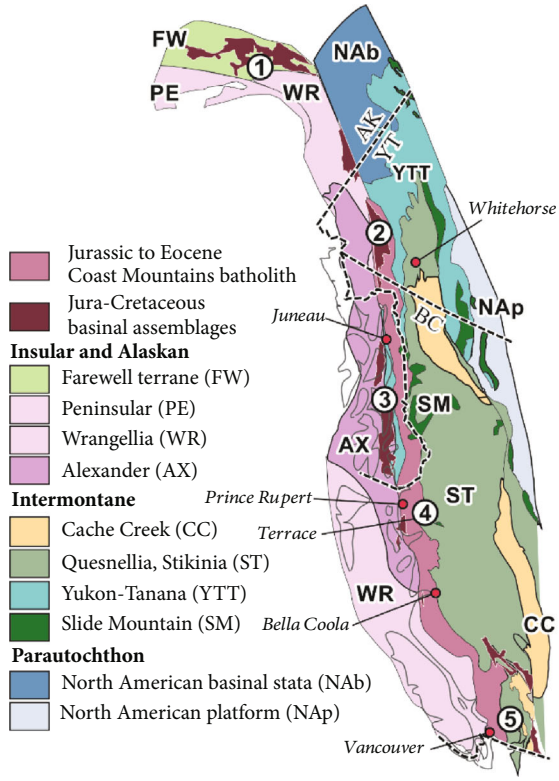

#	Location	Compression + peak metamorphism	Exhumation/ extension	Source
1	S-central Alaska	85–75 Ma		Moore and Box, 2016
2	SW Yukon	82 Ma; **83–76 Ma**	**70 Ma; 63–61 Ma**	Mezger et al., 2001a; lsrael et al., 2011; **this study**
3	SE Alaska: Coast Mountais orogen	90 Ma	85–57 Ma	McClelland and Mattinson, 2000
4	Terrace BC: Central Gneiss Complex	90–70 Ma	70–52 Ma; 55–50 Ma	Rusmore et al., 2005; Andronicos et al., 2003
5	SW BC: Coast Belt thrust system	94–91 Ma		Journeay and Friedman, 1993

FIGURE 11: Terrane map of the western Canadian and Alaskan Cordillera highlighting timing of tectonic events from Alaska to southwestern BC along the Coast Mountains arc. Bold text corresponds to new results from this study. Abbreviations: YT: Yukon Territory; BC; British Columbia; AK: Alaska. Terrane map modified from Israel et al. [30].

constrained orogen-normal structures in southern BC, which are between 94 and 91 Ma [82]. In the Central Gneiss Complex, near Terrace, BC shortening accommodated the burial of basinal rocks enabling the growth of kyanite and garnet from ca. 90 to 70 Ma [21]. Within the Coast Mountains orogen in southeastern Alaska, McClelland and Mattinson [19] also suggest that burial of Gravina belt rocks beneath Yukon-Tanana terrane along the Sumdum fault took place by 90 Ma, not long after the maximum depositional age of the Kluane schist (ca. 95 Ma) [30]. In contrast, similar compressional structures in south-central Alaska in Jura-Cretaceous basinal assemblages appear to be younger, constrained to ca. 85-75 Ma [25], similar to southwest Yukon.

Significant exhumation during the latest Cretaceous similar to that recorded in southwest Yukon is a hallmark of the Central Gneiss Complex in west-central BC south of Terrace [21, 83–86]. Decompression occurred from 70 to 52 Ma as a multistage process that started with slow erosion and coaxial crustal thinning followed by fast near-isothermal decompression and intense heating after the intrusion of the Quotoon pluton at ca. 59 Ma [21]. West of the Central Gneiss Complex, Andronicos et al. [86] suggest that widespread extension occurred from 55 to 50 Ma in the region, with normal faulting beginning as early as 65 Ma [87]. Similarly, along the western Coast Mountains in west-central BC and southeast Alaska between Prince Rupert, BC, and Juneau, Alaska, retrograde metamorphic assemblages, as well as deformation along pluton margins, have been interpreted to be related to periods of Late Cretaceous to Paleogene exhumation (ca. 85-57 Ma; Figure 11) [19]. This exhumation is thought to have occurred along the east side of the Coast shear zone synchronous with pluton emplacement [19, 87, 88].

5.2.3. Correlation with Coast Mountains Orogen and Coast Shear Zone. The foregoing discussion highlights some key similarities that relate to tectonic events recorded along the Insular-Intermontane boundary from Bella Coola, BC, to Juneau, Alaska, and into southwest Yukon (Figure 11). In several locations along this boundary, Late Cretaceous tectonic thickening is associated with high-grade metamorphism followed by latest Cretaceous to Paleogene exhumation and plutonism within the Coast Mountains batholith [19, 21, 79, 87, 88]. Notably, the rocks in southwest Yukon are along strike to the structures observed from Bella Coola, BC, to Juneau, Alaska, that are related to the Coast Mountains orogen (Figures 1 and 11) [19, 21, 88, 89]. These similarities suggest a widespread tectonic event that resulted from the juxtaposition of the Insular and Intermontane terranes. McClelland and Mattinson [19] state that the Coast shear zone ubiquitously separates similar rocks of the Yukon-Tanana terrane or juxtaposes Yukon-Tanana terrane to the east against the Gravina belt and Alexander terrane to the west. Therefore, we propose that the tectonic events recorded in southwest Yukon constrained by this study and described herein represent a northern continuation of the Coast Mountains orogen and the Coast shear zone and support hypotheses of Late Cretaceous to Paleocene crustal thickening and exhumation along the Intermontane-Insular boundary.

5.2.4. Asymmetric Accretion Leading to Diachronous Basinal Collapse. There are two principal and contrasting models to reconcile the accretionary history of the Insular terranes. The first model uses Andean-style tectonics where Middle Jurassic initial accretion of the Insular terranes placed them in an upper plate position along the North American margin. Subsequent southwards sinistral movement of the Insular terranes is thought to have initiated the opening of Jura-Cretaceous intraarc and back-arc pull-apart basins. In this model, mid- to Late Cretaceous shortening caused the collapse of these basins after a transition to more orthogonal convergence and contractional deformation, followed by a dextral transpressional tectonic regime associated with the northward movement and terminal accretion of the Insular terranes [2, 14, 15, 19–25].The second model is based on an archipelago style of accretion with wide ocean basins between the Insular and Intermontane terranes that hosted intraoceanic arc systems bounded by west-dipping subduction and that the Jura-Cretaceous basinal assemblages were deposited in a lower plate position [26, 27]. In this model, protracted westward subduction of 2000-4000 km of oceanic lithosphere under the archipelago outboard of the paleomargin of Laurentia led to the diachronous closure of these intervening basins from the Late Jurassic into the Cretaceous. This model suggests that there was a polarity flip of subduction to (north) eastward, which accompanied Insular terrane accretion from the latest Jurassic into the Eocene, marking the beginning of Andean-style subduction outboard of the Insular terranes [26, 27].

Although there is ongoing debate regarding the pre-Cretaceous interactions (or lack thereof) between the Insular and Intermontane terranes, workers supporting both models agree that by mid- to Late Cretaceous, time thrusting along this margin accompanied by intrusions represents the final collision between the Insular and Intermontane terranes [15, 23]. Despite their differences, both models address a diachronous (final) accretion of the Insular terranes and agree that during the mid- to Late Cretaceous, there was (north) eastward subduction beneath the western margin of Laurentia that accompanied the terminal accretion of the Insular terranes. Irrespective of the model chosen, timing of this episode of (north) eastward subduction and terminal accretion is consistent with petrochronologic results from the Blanchard River assemblage and the other Jura-Cretaceous basinal assemblages within southwest Yukon.

In both models, a dextral transpressional system would have caused the movement of the Insular terranes northwards, gradually and asymmetrically colliding with the western North American margin. This movement of the Insular terranes would cause an asymmetrical collapse of the basinal assemblages juxtaposed between the Insular and Intermontane terranes, initiated in the south and propagated northwards (zippering) into Yukon and south-central Alaska. The gradual northwestward asymmetric collapse, and contraction of the intervening Jura-Cretaceous basins between the Insular and Intermontane terranes offers a mechanism for the somewhat diachronous Late Cretaceous compressional features (ca. 90 Ma in west-central BC vs. 83-76 Ma in southwest Yukon) observed throughout the Northern Canadian and Alaskan Cordillera [14, 15, 19]. In general, an apparent younging of deformation from west-central BC north into Yukon and central Alaska is explained by a continuum of deformation and metamorphism with the northwards movement of the Insular terranes.

6. Conclusions

The Blanchard River assemblage in southwest Yukon belongs to a series of Jura-Cretaceous basinal assemblages juxtaposed between the Insular and Intermontane terranes along much of the length of the Canadian and Alaskan Cordillera. It represents at least a ~5-6 km thick package of metasedimentary rock that has been affected by at least two episodes of deformation and three phases of metamorphism from Late Cretaceous to Paleogene time. Tectonic burial of the Blanchard River assemblage, culminating with peak metamorphism that occurred between ca. 83 and 76 Ma, was in part accompanied by the intrusion of 78-76 Ma orthogneiss. Peak metamorphic conditions within the Blanchard River assemblage reached 635°C-650°C and 6.3-6.7 kbars accompanying penetrative deformation (D_T), which produced southwest-verging isoclinal folds that affected both the Blanchard River assemblage and the overthrusted Yukon-Tanana terrane. Approximately 10-15 km of exhumation of the Blanchard River assemblage occurred at ca. 70-68 Ma, which is recorded by the replacement of garnet, kyanite, and staurolite by lower pressure assemblages that include andalusite, biotite, plagioclase, and spinel. A second phase of deformation (D_{T+1}) is characterized by open, undulating southeast-vergent folds that affect the S_T fabric. D_{T+1} is interpreted to have occurred after the 70-68 Ma exhumation and before the intrusion of the Paleogene Ruby Range suite. A subsequent period of intense heating at ca. 63-61 Ma is indicated by the static overprinting of both prograde (M_{1C}) and retrograde (M_{2C}) metamorphic assemblages with high-temperature sillimanite and cordierite (M_{3C}), which becomes more intense towards the contacts with the Ruby Range suite.

The tectonometamorphic history observed within the Blanchard River assemblage is directly comparable to that recorded in the Kluane schist, a Cretaceous basinal assemblage to the north, where west-directed thrusting of the Yukon-Tanana terrane over the Kluane schist caused intense Late Cretaceous compressional deformation and metamorphism. In both basinal assemblages, tectonic burial was followed by latest Cretaceous exhumation and final contact metamorphism related to the Paleogene intrusion of the Ruby Range suite.

Although the exact nature and initial timing of the accretion of the Insular terranes onto the Laurentian margin remains a contested topic, the Late Cretaceous tectonometamorphism documented herein, which is related to the final collapse of the intervening Jura-Cretaceous basins, marked the terminal accretion of the Insular terranes to the northwestern margin of Laurentia. Similar tectonic events observed in southwest Yukon are also recorded throughout the Coast Mountains of the North American Cordillera in the mid- to Late Cretaceous where the terminal accretion of the Insular terranes onto the western Laurentian margin is attributed to a dextral transpressional regime. A dextral transpressional

system could reconcile seemingly diachronous Late Cretaceous compressional features recorded between the Insular and Intermontane terranes from west-central BC north into Yukon and central Alaska through an asymmetrical collapse of these basins, which was initiated in the south and propagated northwards (zippering) into Yukon and south-central Alaska with a continuum of deformation and metamorphism.

Data Availability

The structural analyses for Blanchard River area; figures of photomicrographs and textural locations of monazite crystals of samples analyzed by in-situ LASS; full suite of U-Th-Pb isotopic analyses, preferred age, and Y-Yb-Lu trace element data for all LASS-ICPMS monazite analyses; and full suite of trace element data for monazite LASS-ICPMS analyses are included within the supplementary information files.

Disclosure

Lianna Vice's present address is Ontario Geological Survey, 933 Ramsey Lake Road, Sudbury, Ontario P3E 6B5. Steve Israel's present address is Archer, Cathro & Associates (1981) Ltd., 41 MacDonald Rd., Whitehorse, Yukon, Y1A 4R1.

Conflicts of Interest

The authors declare no conflict of interest regarding this publication.

Acknowledgments

Funding was provided by grants to Gibson by the Natural Sciences and Engineering Research Council of Canada (NSERC) and Natural Resources Canada Geo-mapping for Energy and Minerals 2 (GEM 2). The authors are grateful to the Yukon Geological Survey for supporting field work and providing data and samples. Mike Jercinovic at UMass is thanked for providing electron microprobe data and monazite maps, and Andrew Kylander-Clark for his support with the LASS-ICPMS analyses at UCSB. We also thank Matt Power and Holly Tutty at SGS for providing QEMSCAN analyses, and Xin Zhang and Matt Bilton at the SFU 4D labs for help with the SEM analyses. Our thanks also extend to Maurice Colpron, Don Murphy, David Moynihan, and Jim Monger for their insightful Cordilleran discussions. Lastly, we would like to thank Luke Beranek and an anonymous reviewer for their constructive reviews which helped to strengthen and add clarity to this contribution, and Tamer Abu-Alam for his deft editorial handling of the manuscript.

Supplementary Materials

Supplementary 1. Structural analyses for Blanchard River area (PDF file).

Supplementary 2. (A–H) Photomicrographs and textural locations of monazite crystals of samples analyzed by in situ LASS (PDF file).

Supplementary 3. (A) The full suite of U-Th-Pb isotopic analyses, preferred age, and Y-Yb-Lu trace element data for all LASS-ICPMS monazite analyses. (B) The full suite of trace element data for monazite LASS-ICPMS analyses (Word Document).

References

[1] P. J. Coney, D. L. Jones, and J. W. H. Monger, "Cordilleran suspect terranes," *Nature*, vol. 288, no. 5789, pp. 329–333, 1980.

[2] J. W. H. Monger, R. A. Price, and D. J. Tempelman-Kluit, "Tectonic accretion and the origin of the two major metamorphic and plutonic welts in the Canadian Cordillera," *Geology*, vol. 10, no. 2, p. 70, 1982.

[3] E. L. Miller, M. M. Miller, C. H. Stevens, J. E. Wright, and R. Madrid, "Late Paleozoic paleogeographic and tectonic evolution of the western U.S. Cordillera,," in *The Cordilleran Orogen: Conterminous U.S*, B. C. Burchfiel, P. W. Lipman, and M. L. Zoroback, Eds., pp. 57–106, Geological Society of America, Boulder, Colorado, 1992.

[4] J. W. H. Monger and R. A. Price, "The Canadian Cordillera: geology and tectonic evolution: Canadian Society of Exploration Geophysicists Recorder," *CSEG Recorder*, vol. 27, pp. 17–36, 2002.

[5] W. R. Dickinson, "Evolution of the North American Cordillera," *Annual Review of Earth and Planetary Sciences*, vol. 32, no. 1, pp. 13–45, 2004.

[6] M. Colpron, J. L. Nelson, and D. C. Murphy, "Northern Cordilleran terranes and their interactions through time," *GSA Today*, vol. 17, no. 4, pp. 4–10, 2007.

[7] L. P. Beranek and J. K. Mortensen, "The timing and provenance record of the Late Permian Klondike orogeny in northwestern Canada and arc-continent collision along western North America," *Tectonics*, vol. 30, no. 5, 2011.

[8] J. L. Nelson, M. Colpron, S. J. Piercey, C. Dusel-Bacon, D. C. Murphy, and C. F. Roots, "Paleozoic tectonic and metallogenetic evolution of pericratonic terranes in Yukon, northern British Columbia and eastern Alaska," in *Paleozoic Evolution and Metallogeny of Pericratonic Terranes at the Ancient Pacific Margin of North America, Canadian and Alaskan Cordillera: Geological Association of Canada Special Paper*, vol. 45, pp. 323–360, Geological Association of Canada, 2006.

[9] J. L. Nelson, M. Colpron, and S. Israel, *The cordillera of British Columbia, Yukon, and Alaska*, Society of Economic Geology, 2013, Special Publication 17.

[10] J. W. H. Monger and H. D. Gibson, "Mesozoic-Cenozoic deformation in the Canadian Cordillera: the record of a "Continental Bulldozer"?," *Tectonophysics*, vol. 757, pp. 153–169, 2019.

[11] W. C. McClelland and G. E. Gehrels, "Geology of the Duncan Canal shear zone; evidence for Early to Middle Jurassic deformation of the Alexander Terrane, southeastern Alaska," *Geological Society of America Bulletin*, vol. 102, no. 10, pp. 1378–1392, 1990.

[12] W. C. McClelland, G. E. Gehrels, and J. B. Saleeby, "Upper Jurassic-Lower Cretaceous basinal strata along the Cordilleran Margin: implications for the accretionary history of the Alexander-Wrangellia-Peninsular Terrane," *Tectonics*, vol. 11, no. 4, pp. 823–835, 1992.

[13] M. G. Mihalynuk, J. Nelson, and L. J. Diakow, "Cache Creek Terrane entrapment; oroclinal paradox within the Canadian Cordillera," *Tectonics*, vol. 13, no. 3, pp. 575–595, 1994.

[14] J. W. H. Monger, P. van der Heyden, J. M. Journeay, C. A. Evenchick, and J. B. Mahoney, "Jurassic-Cretaceous basins along the Canadian Coast Belt; their bearing on pre-mid-Cretaceous sinistral displacements," *Geology*, vol. 22, no. 2, pp. 175–178, 1994.

[15] G. Gehrels, M. Rusmore, G. Woodsworth et al., "U-Th-Pb geochronology of the Coast Mountains batholith in north-coastal British Columbia: Constraints on age and tectonic evolution," *Geological Society of America Bulletin*, vol. 121, no. 9-10, pp. 1341–1361, 2009.

[16] P. van der Heyden, "A Middle Jurassic to early Tertiary Andean-Sierran arc model for the Coast Belt of British Columbia," *Tectonics*, vol. 11, no. 1, pp. 82–97, 1992.

[17] J. B. Saleeby, "Geochronologic investigations along the Alexander-Taku terrane boundary, southern Revillagigedo Island to Cape Fox areas, southeast Alaska, Special Paper 343," in *Tectonics of the Coast Mountains, Southeastern Alaska and British Columbia*, pp. 107–143, Geological Society of America, 2000.

[18] G. E. Gehrels, "Geology of the Chatham Sound region, Southeast Alaska and coastal British Columbia," *Canadian Journal of Earth*, vol. 38, no. 11, pp. 1579–1599, 2001.

[19] W. C. McClelland and J. M. Mattinson, "Cretaceous-tertiary evolution of the western Coast Mountains, central Southeastern Alaska," *Geological Society of America, Special Paper*, vol. 343, pp. 159–182, 2000.

[20] K. D. Ridgway, J. M. Trop, W. J. Nokleberg, C. M. Davidson, and K. R. Eastham, "Mesozoic and Cenozoic tectonics of the eastern and central Alaska Range; progressive basin development and deformation in a suture zone," *Geological Society of America Bulletin*, vol. 114, no. 12, pp. 1480–1504, 2002.

[21] M. E. Rusmore, G. J. Woodsworth, and G. E. Gehrels, "Two-stage exhumation of midcrustal arc rocks, Coast Mountains, British Columbia," *Tectonics*, vol. 24, no. 5, 2005.

[22] J. M. Trop and K. D. Ridgway, "Mesozoic and Cenozoic tectonic growth of southern Alaska; a sedimentary basin perspective," in *Special Paper 431: Tectonic Growth of a Collisional Continental Margin: Crustal Evolution of Southern Alaska*, vol. 431, pp. 55–94, Geological Society of America, 2007.

[23] B. A. Hampton, K. D. Ridgway, and G. E. Gehrels, "A detrital record of Mesozoic island arc accretion and exhumation in the North American Cordillera; U/Pb geochronology of the Kahiltna Basin, southern Alaska," *Tectonics*, vol. 29, no. 4, 2010.

[24] C. P. Hults, F. H. Wilson, R. A. Donelick, and P. B. O'Sullivan, "Two flysch belts having distinctly different provenance suggest no stratigraphic link between the Wrangellia composite terrane and the paleo-Alaskan margin," *Lithosphere*, vol. 5, no. 6, pp. 575–594, 2013.

[25] T. E. Moore and S. E. Box, "Age, distribution and style of deformation in Alaska north of 60°N: implications for assembly of Alaska," *Tectonophysics*, vol. 691, pp. 133–170, 2016.

[26] K. Sigloch and M. G. Mihalynuk, "Intra-oceanic subduction shaped the assembly of Cordilleran North America," *Nature*, vol. 496, no. 7443, pp. 50–56, 2013.

[27] K. Sigloch and M. G. Mihalynuk, "Mantle and geological evidence for a late Jurassic – cretaceous suture spanning North America," *Geological Society of America Bulletin*, vol. 129, no. 11-12, pp. 1489–1520, 2017.

[28] G. E. Gehrels, W. C. McClelland, S. D. Samson, P. J. Patchett, and M. J. Orchard, "Geology of the western flank of the Coast Mountains between Cape Fanshaw and Taku Inlet, Southeastern Alaska," *Tectonics*, vol. 11, no. 3, pp. 567–585, 1992.

[29] C. A. Evenchick, "Northeast-trending folds in the western Skeena Fold Belt, northern Canadian Cordillera: a record of Early Cretaceous sinistral plate convergence," *Journal of Structural Geology*, vol. 23, no. 6-7, pp. 1123–1140, 2001.

[30] S. Israel, D. Murphy, V. Bennett, J. Mortensen, and J. Crowley, "New insights into the geology and mineral potential of the Coast Belt in southwestern Yukon," in *Yukon Exploration and Geology 2010*, K. E. MacFarlane, L. H. Weston, C. Relf, M. G. Nordling, and P. J. Sack, Eds., pp. 101–123, Yukon Geological Survey, 2011.

[31] E. Bordet, S. Israel, and D. Moynihan, "Geology of the Takhanne River (NTS 115A/2) and Kluhini River (115A/7) map areas, Southwest Yukon," in *Yukon Exploration and Geology 2014*, pp. 1–16, Yukon Geological Survey, 2015.

[32] L. Vice, *Late cretaceous to Paleocene evolution of the Blanchard River assemblage, southwest Yukon; implications for Mesozoic accretionary processes in the northwestern Cordillera, [M.S. Thesis]*, Simon Fraser University, Burnaby, BC, 2017.

[33] G. H. Eisbacher, "Sedimentology of the Dezadeash flysch and its implications for strike-slip faulting along the Denali Fault, Yukon Territory and Alaska," *Canadian Journal of Earth Sciences*, vol. 13, no. 11, pp. 1495–1513, 1976.

[34] J. E. Mezger, T. Chacko, and P. Erdmer, "Metamorphism at a late Mesozoic accretionary margin: a study from the Coast Belt of the North American Cordillera," *Journal of Metamorphic Geology*, vol. 19, no. 2, pp. 121–137, 2001.

[35] J. E. Mezger, R. A. Creaser, P. Erdmer, and S. T. Johnston, "A cretaceous back-arc basin in the Coast Belt of the northern Canadian Cordillera: evidence from geochemical and neodymium isotope characteristics of the Kluane metamorphic assemblage, Southwest Yukon," *Canadian Journal of Earth*, vol. 38, no. 1, pp. 91–103, 2001.

[36] G. W. Lowey, "Lithofacies analysis of the Dezadeash Formation (Jura-Cretaceous), Yukon, Canada: The depositional architecture of a mud/sand-rich turbidite system," *Sedimentary Geology*, vol. 198, no. 3-4, pp. 273–291, 2007.

[37] M. Colpron, J. L. Nelson, and D. C. Murphy, "A tectonostratigraphic framework for the pericratonic terranes of the northern Canadian Cordillera," in *Geological Association of Canada, Special Paper*, vol. 45, pp. 1–23, Geological Association of Canada, 2006.

[38] D. C. Murphy, P. van der Heyden, R. R. Parrish et al., "New geochronological constraints on Jurassic deformation of the western edge of North America, southeastern Canadian Cordillera," in *Geological Society of America Special Paper*, vol. 299, pp. 159–171, Geological Society of America, 1995.

[39] C. Dusel-Bacon, M. A. Lanphere, W. D. Sharp, P. W. Layer, and V. L. Hansen, "Mesozoic thermal history and timing of structural events for the Yukon-Tanana Upland, East-Central Alaska; 40Ar/ 39Ar data from metamorphic and plutonic rocks," *Canadian Journal of Earth Sciences*, vol. 39, no. 6, pp. 1013–1051, 2002.

[40] R. G. Berman, J. J. Ryan, S. P. Gordey, and M. Villeneuve, "Permian to Cretaceous polymetamorphic evolution of the Stewart River region, Yukon-Tanana terrane, Yukon, Canada:P-Tevolution linked within situSHRIMP monazite geochronology," *Journal of Metamorphic Geology*, vol. 25, no. 7, pp. 803–827, 2007.

[41] R. D. Staples, H. D. Gibson, R. G. Berman, J. J. Ryan, and M. Colpron, "A window into the early to mid-cretaceous

infrastructure of the Yukon-Tanana terrane recorded in multistage garnet of west-central Yukon, Canada," *Journal of Metamorphic Geology*, vol. 31, no. 7, pp. 729–753, 2013.

[42] R. D. Staples, D. C. Murphy, H. D. Gibson, M. Colpron, R. G. Berman, and J. J. Ryan, "Middle Jurassic to earliest Cretaceous mid-crustal tectono-metamorphism in the northern Canadian Cordillera: Recording foreland-directed migration of an orogenic front," *Geological Society of America Bulletin*, vol. 126, no. 11-12, pp. 1511–1530, 2014.

[43] R. Staples, H. D. Gibson, M. Colpron, and J. J. Ryan, "An orogenic wedge model for diachronous deformation, metamorphism, and exhumation in the hinterland of the northern Canadian Cordillera," *Lithosphere*, vol. 8, no. 2, pp. 165–184, 2016.

[44] A. D. Clark, *Tectonometamorphic history of mid-crustal rocks at Aishihik Lake, southwest Yukon, [M.S. thesis]*, Simon Fraser University, Burnaby, BC, 2017.

[45] L. P. Beranek, C. R. van Staal, W. C. McClelland, S. Israel, and M. G. Mihalynuk, "Detrital zircon Hf isotopic compositions indicate a northern Caledonian connection for the Alexander Terrane," *Lithosphere*, vol. 5, no. 2, pp. 163–168, 2013.

[46] R. Cobbett, S. Israel, J. Mortensen, N. Joyce, and J. Crowley, "Structure and kinematic evolution of the Duke River fault, southwestern Yukon," *Canadian Journal of Earth Sciences*, vol. 54, no. 3, pp. 322–344, 2017.

[47] D. L. Jones, N. J. Silberling, and J. Hillhouse, "Wrangellia—a displaced terrane in northwestern North America," *Canadian Journal of Earth*, vol. 14, no. 11, pp. 2565–2577, 1977.

[48] N. W. D. Massey, *Geology and Mineral Resources of the Duncan Sheet, Vancouver Island 92B/13*, no. article 02269430, 1995Province of British Columbia, Ministry of Energy, Mines and Petroleum Resources, Victoria, BC, Canada, 1995.

[49] C. J. Yorath, A. Sutherland Brown, and N. W. D. Massey, *LITHOPROBE, southern Vancouver Island, British Columbia: Geology*, Geological Survey of Canada, Bulletin 498, 1999.

[50] M. C. Gardner, S. C. Bergman, G. W. Cushing et al., "Pennsylvanian pluton stitching of Wrangellia and the Alexander Terrane, Wrangell Mountains, Alaska," *Geology*, vol. 16, no. 11, pp. 967–971, 1988.

[51] S. Israel, L. Beranek, R. M. Friedman, and J. L. Crowley, "New ties between the Alexander terrane and Wrangellia and implications for North America Cordilleran evolution," *Lithosphere*, vol. 6, no. 4, pp. 270–276, 2014.

[52] G. W. Lowey, "A new estimate of the amount of displacement on the Denali Fault system based on the occurrence of carbonate megaboulders in the Dezadeash formation (Jura-cretaceous), Yukon, and the Nutzotin Mountains sequence (Jura-Cretaceous), Alaska," *Bulletin of Canadian Petroleum Geology*, vol. 46, no. 3, pp. 379–386, 1998.

[53] D. C. Murphy, J. K. Mortensen, and C. van Staal, "Windy-McKinley Terrane, western Yukon and eastern Alaska; terrane analysis returns to its roots," *Geological Society of America, Abstracts with Programs*, vol. 41, no. 5, pp. 10–10, 2008.

[54] S. Israel, M. Colpron, J. Cubley, D. Moynihan, D. C. Murphy, and C. Relf, "The Bear Creek assemblage: a latest Triassic volcano-sedimentary succession in southwest Yukon," in *Yukon Exploration and Geology 2014*, K. E. MacFarlane, M. G. Nordling, and P. J. Sack, Eds., pp. 99–112, Yukon Geological Survey, 2015.

[55] G. W. Lowey, "Provenance analysis of the Dezadeash formation (Jurassic–Cretaceous), Yukon, Canada: implications regarding a linkage between the Wrangellia composite terrane and the western margin of Laurasia," *Canadian Journal of Earth Sciences*, vol. 56, no. 1, pp. 77–100, 2019.

[56] G. J. Woodsworth, R. G. Anderson, and R. L. Armstrong, "Chapter 15: Plutonic Regimes," in *Geology of the Cordilleran Orogen in Canada*, H. Gabrielse and C. J. Yorath, Eds., pp. 491–531, Geological Survey of Canada, 1991, Geology of Canada, no. 4.

[57] S. Israel, M. Friend, and A. Borch, "Preliminary report on the bedrock geology of the Long Lake and Moraine Lake areas, southwestern Yukon (NTS 115A/15 and 115H/2 and 7)," in *Yukon Exploration and Geology 2016*, K. E. MacFarlane and L. H. Weston, Eds., pp. 87–102, Yukon Geological Survey, 2016.

[58] M. Colpron, S. Israel, and M. Friend, *Yukon Plutonic Suites*, Yukon Geological Survey, 2016, Open File 2016-37, scale 1:750000.

[59] G. W. Lowey, "The Tatshenshini shear zone (new) in southwestern Yukon, Canada: Comparison with the Coast shear zone in British Columbia and southeastern Alaska and implications regarding the Shakwak suture," *Tectonics*, vol. 19, no. 3, pp. 512–528, 2000.

[60] D. Pirrie, A. R. Butcher, M. R. Power, P. Gottlieb, and G. L. Miller, "Rapid quantitative mineral and phase analysis using automated scanning electron microscopy (QemSCAN); potential applications in forensic geoscience," *Geological Society Special Publications*, vol. 232, no. 1, pp. 123–136, 2004.

[61] G. Foster, P. Kinny, D. Vance, C. Prince, and N. Harris, "The significance of monazite U-Th-Pb age data in metamorphic assemblages; a combined study of monazite and garnet chronometry," *Earth and Planetary Science Letters*, vol. 181, no. 3, pp. 327–340, 2000.

[62] J. M. Pyle, F. S. Spear, R. L. Rudnick, and W. F. McDonough, "Monazite-xenotime-garnet equilibrium in metapelites and a new monazite-garnet thermometer," *Journal of Petrology*, vol. 42, no. 11, pp. 2083–2107, 2001.

[63] G. Foster, H. D. Gibson, R. Parrish, M. Horstwood, J. Fraser, and A. Tindle, "Textural, chemical and isotopic insights into the nature and behaviour of metamorphic monazite," *Chemical Geology*, vol. 191, no. 1-3, pp. 183–207, 2002.

[64] H. D. Gibson, S. D. Carr, R. L. Brown, and M. A. Hamilton, "Correlations between chemical and age domains in monazite, and metamorphic reactions involving major pelitic phases: an integration of ID-TIMS and SHRIMP geochronology with Y-Th-U X-ray mapping," *Chemical Geology*, vol. 211, no. 3-4, pp. 237–260, 2004.

[65] A. R. C. Kylander-Clark, B. R. Hacker, and J. M. Cottle, "Laser-ablation split-stream ICP petrochronology," *Chemical Geology*, vol. 345, pp. 99–112, 2013.

[66] R. A. Stern and R. G. Berman, "Monazite U-Pb and Th-Pb geochronology by ion microprobe, with an application to in situ dating of an Archean metasedimentary rock," *Chemical Geology*, vol. 172, no. 1-2, pp. 113–130, 2001.

[67] T. R. Ireland and G. M. Gibson, "SHRIMP monazite and zircon geochronology of high-grade metamorphism in New Zealand," *Journal of Metamorphic Geology*, vol. 16, no. 2, pp. 149–167, 1998.

[68] U. Schärer, "The effect of initial^{230}Th disequilibrium on young UPb ages: the Makalu case, Himalaya," *Earth and Planetary Science Letters*, vol. 67, no. 2, pp. 191–204, 1984.

[69] R. R. Parrish, "U-Pb dating of monazite and its application to geological problems," *Canadian Journal of Earth Sciences*, vol. 27, no. 11, pp. 1431–1450, 1990.

[70] D. J. Cherniak, E. B. Watson, M. Grove, and T. M. Harrison, "Pb diffusion in monazite: a combined RBS/SIMS study[1]," *Geochimica et Cosmochimica Acta*, vol. 68, no. 4, pp. 829–840, 2004.

[71] E. Gardés, O. Jaoul, J.-M. Montel, A.-M. Seydoux-Guillaume, and R. Wirth, "Pb diffusion in monazite; an experimental study of $Pb^{2+} + Th^{4+} \Leftrightarrow 2Nd^{3+}$ interdiffusion," *Geochimica et Cosmochimica Acta*, vol. 70, no. 9, pp. 2325–2336, 2006.

[72] J. T. Stacey and J. D. Kramers, "Approximation of terrestrial lead isotope evolution by a two-stage model," *Earth and Planetary Science Letters*, vol. 26, no. 2, pp. 207–221, 1975.

[73] P. Štipska, R. Powell, R. W. White, and J. A. Baldwin, "Using calculated chemical potential relationships to account for coronas around kyanite: an example from the Bohemian Massif," *Journal of Metamorphic Geology*, vol. 28, no. 1, pp. 97–116, 2010.

[74] J. A. Baldwin, R. Powell, R. W. White, and P. Štípská, "Using calculated chemical potential relationships to account for replacement of kyanite by symplectite in high pressure granulites," *Journal of Metamorphic Geology*, vol. 33, no. 3, pp. 311–330, 2015.

[75] F. S. Spear, *Metamorphic phase equilibria and pressure-temperature-time paths*, Mineralogical Society of America, 1995.

[76] U. Ring, M. T. Brandon, S. D. Willett, and G. S. Lister, "Exhumation processes," in *Exhumation Processes: Normal Faulting, Ductile Flow, and Erosion*, U. Ring, M. T. Brandon, G. S. Lister, and S. D. Willett, Eds., vol. 154, no. 1pp. 1–27, Geol. Soc. London Spec. Publ, 1999.

[77] J. E. Mezger, *Tectonometamorphic evolution of the Kluane metamorphic assemblage, SW Yukon: evidence for late cretaceous eastward subduction of oceanic crust underneath North America, [Ph.D. thesis]*, University of Alberta, Edmonton, AB, 1997.

[78] P. Erdmer and J. K. Mortensen, "A 1200-km-long Eocene metamorphic-plutonic belt in the northwestern Cordillera: evidence from southwest Yukon," *Geology*, vol. 21, no. 11, article 10391042, 1993.

[79] M. L. Crawford, L. S. Hollister, and G. J. Woodsworth, "Crustal deformation and regional metamorphism across a terrane boundary, Coast Plutonic Complex, British Columbia," *Tectonics*, vol. 6, no. 3, pp. 343–361, 1987.

[80] C. A. Evenchick, "Geometry, evolution, and tectonic framework of the Skeena fold belt, north central British Columbia," *Tectonics*, vol. 10, no. 3, pp. 527–546, 1991.

[81] M. E. Rusmore and G. J. Woodsworth, "Coast plutonic complex: a mid-Cretaceous contractional orogen," *Geology*, vol. 19, no. 9, pp. 941–944, 1991.

[82] J. M. Journeay and R. M. Friedman, "The Coast Belt thrust system; evidence of Late Cretaceous shortening in Southwest British Columbia," *Tectonics*, vol. 12, no. 3, pp. 756–775, 1993.

[83] L. S. Hollister, "Metamorphic evidence for rapid (2 mm/yr) uplift of a portion of the Central Gneiss Complex, Coast Mountains, BC," *The Canadian Mineralogist*, vol. 20, no. 3, pp. 319–332, 1982.

[84] C. L. Andronicos, L. S. Hollister, C. Davidson, and D. Chardon, "Kinematics and tectonic significance of transpressive structures within the Coast Plutonic Complex, British Columbia," *Journal of Structural Geology*, vol. 21, no. 2, pp. 229–243, 1999.

[85] C. L. Andronicos, *Tectonic evolution of the Coast plutonic complex, [Ph.D. thesis]*, Princeton University, Princeton, NJ, 1999.

[86] C. L. Andronicos, D. H. Chardon, L. S. Hollister, G. E. Gehrels, and G. J. Woodsworth, "Strain partitioning in an obliquely convergent orogen, plutonism, and synorogenic collapse: Coast Mountains Batholith, British Columbia, Canada," *Tectonics*, vol. 22, no. 2, 2003.

[87] M. L. Crawford, K. A. Klepeis, G. Gehrels, and C. Isachsen, "Batholith emplacement at mid-crustal levels and its exhumation within an obliquely convergent margin," *Tectonophysics*, vol. 312, no. 1, pp. 57–78, 1999.

[88] M. E. Rusmore, G. Gehrels, and G. J. Woodsworth, "Southern continuation of the coast shear zone and Paleocene strain partitioning in British Columbia–southeast Alaska," *Geological Society of America Bulletin*, vol. 113, no. 8, pp. 961–975, 2001.

[89] M. E. Rusmore, G. J. Woodsworth, and G. E. Gehrels, "Late Cretaceous evolution of the eastern Coast Mountains, Bella Coola, British Columbia," in *Tectonics of the Coast Mountains, Southeastern Alaska and British Columbia: Boulder, Colorado*, H. H. Stowell and W. C. McClelland, Eds., vol. 343, Geological Society of America, 1994.